Journal of Sound and Vibration 330 (2011) 194–216

Contents lists available at ScienceDirect

Journal of Sound and Vibration

journal homepage: www.elsevier.com/locate/jsvi

Modeling and analysis of laminate composite plates with embedded active–passive piezoelectric networks

Tatiane Corrêa de Godoy, Marcelo Areias Trindade *

Department of Mechanical Engineering, São Carlos School of Engineering, University of São Paulo, Av. Trabalhador São-Carlense, 400, São Carlos, SP 13566-590, Brazil

ARTICLE INFO

Article history:
Received 22 December 2009
Received in revised form
5 July 2010
Accepted 4 August 2010
Handling Editor: K. Worden
Available online 9 September 2010

ABSTRACT

The objective of this work is to present the finite element modeling of laminate composite plates with embedded piezoelectric patches or layers that are then connected to active–passive resonant shunt circuits, composed of resistance, inductance and voltage source. Applications to passive vibration control and active control authority enhancement are also presented and discussed. The finite element model is based on an equivalent single layer theory combined with a third-order shear deformation theory. A stress-voltage electromechanical model is considered for the piezoelectric materials fully coupled to the electrical circuits. To this end, the electrical circuit equations are also included in the variational formulation. Hence, conservation of charge and full electromechanical coupling are guaranteed. The formulation results in a coupled finite element model with mechanical (displacements) and electrical (charges at electrodes) degrees of freedom. For a Graphite-Epoxy (Carbon-Fibre Reinforced) laminate composite plate, a parametric analysis is performed to evaluate optimal locations along the plate plane (xy) and thickness (z) that maximize the effective modal electromechanical coupling coefficient. Then, the passive vibration control performance is evaluated for a network of optimally located shunted piezoelectric patches embedded in the plate, through the design of resistance and inductance values of each circuit, to reduce the vibration amplitude of the first four vibration modes. A vibration amplitude reduction of at least 10 dB for all vibration modes was observed. Then, an analysis of the control authority enhancement due to the resonant shunt circuit, when the piezoelectric patches are used as actuators, is performed. It is shown that the control authority can indeed be improved near a selected resonance even with multiple pairs of piezoelectric patches and active–passive circuits acting simultaneously.

1. Introduction

In the past two decades, piezoelectric materials have been widely used as distributed sensors and actuators for structural vibration control [1]. In particular, piezoelectric ceramics, such as the lead titanate zirconate (PZT) family of ceramics, are interesting choices for integrated sensors and actuators since they can be found in the form of small and thin patches and, hence, may be bonded to or embedded in laminate composite structures leading to little structural modification combined to a relatively high electromechanical coupling. Patches made of piezoelectric macro-fibre

* Corresponding author.
E-mail addresses: tcgodoy@sc.usp.br (T.C. Godoy), trindade@sc.usp.br (M.A. Trindade).

0022-460X/$ - see front matter © 2010 Elsevier Ltd. All rights reserved.
doi:10.1016/j.jsv.2010.08.010

composites (MFC) can be another interesting choice for this type of applications. The piezoelectric effect of embedded PZT patches may then be used to estimate local deformation/vibration of the structure by means of an electric voltage/charge measurement in the PZT (direct or sensor effect) and/or induce local deformation/vibration of the structure by applying an electric voltage/charge to the PZT (inverse or actuator effect) [2,3]. Therefore, depending on the electronics connected to the piezoelectric transducers, the vibration control can be passive, active or hybrid active–passive [4]. Passive control is particularly interesting since there is no need to inject additional energy into the system so that the mechanical energy dissipation is due only to transformation into electrical energy and heat [5,6]. The idea of using shunted piezoelectric materials is based on the important electromechanical coupling it provides, converting part of the vibratory energy into electrical energy which is then dissipated through the shunt circuit [6].

More recently, research was redirected to combine active and passive vibration control techniques [7]. One of these techniques, the so-called Active–Passive Piezoelectric Networks (APPN), integrates an active voltage source with a passive resistance–inductance shunt circuit to a piezoelectric sensor/actuator [8]. In this case, the piezoelectric material serves two purposes. First, the vibration strain energy of the structure can be transferred to the shunt circuit, through the difference of electric potential induced in the piezoelectric material electrodes, and then passively dissipated in the electric components of the shunt circuit [5,6]. On the other hand, the piezoelectric material may also serve as an actuator for which a control voltage can be applied to actively control the structural vibrations. This technique allows to simultaneously dissipate passively vibratory energy through the shunt circuit and actively control the structural vibrations. It has been shown that combined active–passive vibration control allows better performance with smaller cost than separate active and passive control, provided the simultaneous action is optimized [8].

In order to better understand the electromechanical interaction between piezoelectric sensors and actuators and vibrating structures, several research groups have focused on proposing and implementing modeling techniques for structures containing piezoelectric elements. In particular, usual modeling techniques for laminate structures were adapted and extended to include the piezoelectric effect [9]. There are today several modeling techniques for laminate structures available that include piezoelectric elements. Most of them can be grouped into: (i) three-dimensional elasticity theories, (ii) two-dimensional equivalent single layer theories, and (iii) discrete-layer or layerwise theories. Both analytical and numerical methods can be applied to approximate the solutions of the equations resulting from these models [10,11].

Three-dimensional theories are evidently more accurate since there is no need to make approximations for the mechanical and electrical fields. However, except for the case of simplified boundary conditions, an analytical solution cannot be found and one must search for a numerical approximation, for which a series of simplifying assumptions must be included for the discretization. Although some authors focused on analytical solutions for three-dimensional models of laminate plates with piezoelectric layers [12], most three-dimensional models were combined to the finite element method for approximate solutions [13]. Most three-dimensional analysis of laminate plates with piezoelectric elements were limited to thin piezoelectric layers in the extension mode, that is poled in the thickness direction. More recently, Baillargeon and Vel [14] and Deü and Benjeddou [15] used three-dimensional theories to model laminate plates with embedded piezoelectric materials in the shear mode, that is poled in the length/width direction.

Two-dimensional equivalent single layer theories yield equations of motion that are easier to solve but also contain a series of simplifying assumptions. In particular, some a priori assumptions for the kinematics along the thickness direction must be made. For that, there have been a number of propositions presented in the literature, imposing polynomial functions of different orders or piecewise continuous (zig-zag) functions to interpolate the kinematics behavior across the thickness [16]. Reddy [17] proposed a finite element formulation and Navier solutions for simply supported plates with thickness-poled piezoelectric sensors and actuators using equivalent single layer combined to classical laminated plate (CLPT), first-order shear (FSDT) and third-order shear (TSDT) deformation theories. TSDT theory was also used recently to model the shear piezoelectric core layer of a sandwich beam structure [18,19]. For laminated plates with shear piezoelectric materials, Aldraihem and Khdeir [20] presented an equivalent single layer model using FSDT and TSDT.

Layerwise theories allow two-dimensional modeling of the kinematics as equivalent single layer theories, but with independent sets of variables for each constitutive layer. Therefore, they provide a more kinematically correct through-thickness representation. However, for practical laminate structures, they also lead to a great number of independent variables meaning a high computational cost to solve the equations. Saravanos et al. [9] and Benjeddou and Deü [21], among others, considered a layerwise model for laminate plates with piezoelectric elements.

In order to study laminate plates with piezoelectric materials connected to active and passive shunt circuits, it is necessary to account for the coupling between piezoelectric elements and external circuits. There are mainly two techniques used in the literature to perform that task. The first consists in modifying the equivalent piezoelectric element impedance considering the piezoelectric element, in unidirectional deformation, and electric circuit as impedances in parallel for which the admittance can be summed. This leads to a modification in the constitutive equations for the piezoelectric material and, in particular, its elastic coefficient becomes a function of the circuit impedance [6]. A second approach considers the equivalence between the charge generated/induced in the piezoelectric material electrodes and the charge flowing in the electric circuit to which it is connected. This allows to write independently the equations of motion for the structure with piezoelectric elements and the electric circuit before coupling the charge variables [22,23]. Unlike the first one, this technique allows a time-domain analysis and does not require unidirectional deformation in the piezoelectric material.

The objective of this work is to present the finite element modeling of laminate composite plates with embedded piezoelectric patches or layers that are then connected to active–passive resonant shunt circuits, composed of resistance, inductance and voltage source. The model is based on an equivalent single layer theory combined with TSDT. A stress-voltage electromechanical model is considered for the piezoelectric materials fully coupled to the electric circuit. To this end, the electric circuits equations are also included in the variational formulation. Hence, conservation of charge and full electromechanical coupling are guaranteed. The formulation results in a coupled finite element model with mechanical (displacements) and electrical (charges at electrodes) degrees of freedom. For a Graphite-Epoxy (Carbon-Fibre Reinforced) laminate composite plate, a parametric analysis is performed to evaluate optimal locations along the plate plane (xy) and thickness (z) that maximize the effective modal electromechanical coupling coefficient. Then, the passive vibration control performance is evaluated for a network of optimally located shunted piezoelectric patches embedded in the plate, through the design of resistance and inductance values of each circuit, to reduce the vibration amplitude of the first four vibration modes. Then, an analysis of the control authority enhancement, when the piezoelectric patches are used as actuators, due to the resonant shunt circuit is performed.

2. Finite element model

A laminated plate composed of elastic and piezoelectric layers is considered. Both elastic and piezoelectric layers are supposed to be thin, such that a plane stress state can be assumed, perfectly bonded and made of orthotropic piezoelectric materials. Elastic layers are obtained by setting their piezoelectric coefficients to zero. Upper and lower surfaces of piezoelectric layers are assumed to be fully covered by electrodes. The equivalent single layer theory is used so that the same displacement field is considered for all $2n$ layers of the laminate plate. Also, for simplifying purposes, only symmetric laminate plates are considered, however the electric displacements in each layer are independent.

2.1. Mechanical displacements and strains

The displacement fields for the laminate plate are defined according to a third-order shear deformation theory (TSDT) proposed by Reddy [17], such that

$$u(x,y,z,t) = u_0(x,y,t) + z\psi_x(x,y,t) - c_1 z^3[\psi_x(x,y,t) + w_{0,x}(x,y,t)],$$

$$v(x,y,z,t) = v_0(x,y,t) + z\psi_y(x,y,t) - c_1 z^3[\psi_y(x,y,t) + w_{0,y}(x,y,t)],$$

$$w(x,y,z,t) = w_0(x,y,t), \tag{1}$$

where u_0, v_0 and w_0 are the displacements and ψ_x and ψ_y are the cross-section rotations at the neutral surface ($z=0$) of the laminate plate. $w_{0,x}$ and $w_{0,y}$ are the derivatives of w_0 in x- and y-directions, respectively. c_1 is a constant that allows FSDT ($c_1=0$) or TSDT ($c_1=4/3h^2$) to be implemented (Fig. 1).

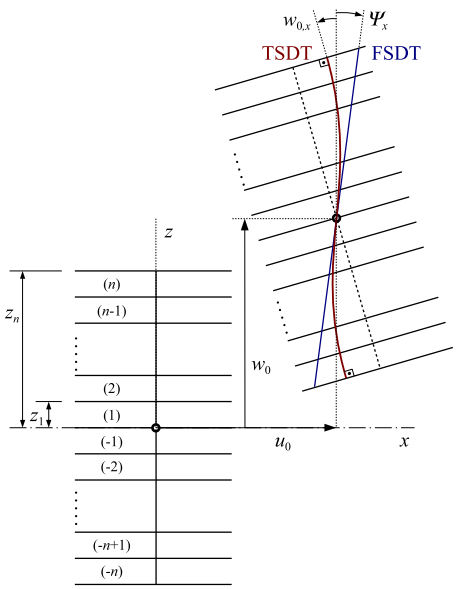

Fig. 1. Representation of the assumed kinematics for FSDT and TSDT.

Considering the standard relations between displacements and infinitesimal strains yields the following strain components:

$$\varepsilon_1 = \varepsilon_1^0 + z\varepsilon_1^1 - c_1 z^3 \varepsilon_1^3, \quad \varepsilon_2 = \varepsilon_2^0 + z\varepsilon_2^1 - c_1 z^3 \varepsilon_2^3,$$

$$\varepsilon_3 = 0, \quad \varepsilon_4 = \varepsilon_4^0 - 3c_1 z^2 \varepsilon_4^2,$$

$$\varepsilon_5 = \varepsilon_5^0 - 3c_1 z^2 \varepsilon_5^2, \quad \varepsilon_6 = \varepsilon_6^0 + z\varepsilon_6^1 - c_1 z^3 \varepsilon_6^3, \tag{2}$$

where generalized strains are defined as

$$\varepsilon_1^0 = u_{0,x},\ \varepsilon_1^1 = \psi_{x,x}, \quad \varepsilon_1^3 = (\psi_{x,x} + w_{0,xx}),$$

$$\varepsilon_2^0 = v_{0,y},\ \varepsilon_2^1 = \psi_{y,y}, \quad \varepsilon_2^3 = (\psi_{y,y} + w_{0,yy}),$$

$$\varepsilon_6^0 = (u_{0,y} + v_{0,x}), \quad \varepsilon_6^1 = (\psi_{x,y} + \psi_{y,x}),$$

$$\varepsilon_6^3 = (\psi_{x,y} + \psi_{y,x} + 2w_{0,xy}),$$

$$\varepsilon_4^0 = \varepsilon_4^2 = (\psi_y + w_{0,y}), \quad \varepsilon_5^0 = \varepsilon_5^2 = (\psi_x + w_{0,x}). \tag{3}$$

2.2. Piezoelectric constitutive equations

Linear orthotropic piezoelectric materials with material symmetry axes parallel to the plate ones are considered here. c_{ij}^D, h_{kj} and β_{kl}^ε ($i,j=1,\ldots,6$; $k,l=1,\ldots,3$) denote their elastic (for constant electric displacement), piezoelectric and dielectric (for constant strain) material constants. The potential energy of a given piezoelectric layer can be described by its electric enthalpy density [22,23]

$$U(\boldsymbol{\varepsilon},\mathbf{D}) = \frac{1}{2}\boldsymbol{\varepsilon}^{\mathrm{t}}\mathbf{c}^D\boldsymbol{\varepsilon} - \boldsymbol{\varepsilon}^{\mathrm{t}}\mathbf{h}^{\mathrm{t}}\mathbf{D} + \frac{1}{2}\mathbf{D}^{\mathrm{t}}\boldsymbol{\beta}^\varepsilon\mathbf{D}. \tag{4}$$

The constitutive equations of each piezoelectric layer are obtained from $\boldsymbol{\sigma} = \partial U(\boldsymbol{\varepsilon},\mathbf{D})/\partial\boldsymbol{\varepsilon}$ and $\mathbf{E} = \partial U(\boldsymbol{\varepsilon},\mathbf{D})/\partial\mathbf{D}$ that are

$$\boldsymbol{\sigma} = \mathbf{c}^D\boldsymbol{\varepsilon} - \mathbf{h}^{\mathrm{t}}\mathbf{D}, \quad \mathbf{E} = -\mathbf{h}\boldsymbol{\varepsilon} + \boldsymbol{\beta}^\varepsilon\mathbf{D}. \tag{5}$$

The material constants $\mathbf{c}^D$, $\mathbf{h}$ and $\boldsymbol{\beta}^\varepsilon$ can be obtained from the standard strain-charge form (d-form) constants, $\mathbf{s}^E$, $\mathbf{d}$ and $\boldsymbol{\varepsilon}^\sigma$, using the following transformations: $\mathbf{h} = (\boldsymbol{\varepsilon}^\varepsilon)^{-1}\mathbf{d}(\mathbf{s}^E)^{-1}$, $\mathbf{c}^D = (\mathbf{s}^E)^{-1}$ $[\mathbf{I} + \mathbf{d}\mathbf{h}^{\mathrm{t}}]$ and $\boldsymbol{\beta}^\varepsilon = (\boldsymbol{\varepsilon}^\varepsilon)^{-1}$, where $\boldsymbol{\varepsilon}^\varepsilon = \boldsymbol{\varepsilon}^\sigma - \mathbf{d}(\mathbf{s}^E)^{-1}\mathbf{d}^{\mathrm{t}}$.

For thin layers fully covered with electrodes on their upper and lower surfaces, plane stress, $\sigma_3 = 0$, and unidirectional electric displacement, $D_1 = D_2 = 0$, hypotheses can be considered. Hence, the previously presented constitutive equations can be reduced to

$$\begin{Bmatrix} \sigma_1 \\ \sigma_2 \\ \sigma_4 \\ \sigma_5 \\ \sigma_6 \\ E_3 \end{Bmatrix} = \begin{bmatrix} \overline{c}_{11}^D & \overline{c}_{12}^D & 0 & 0 & 0 & -\overline{h}_{31} \\ \overline{c}_{12}^D & \overline{c}_{22}^D & 0 & 0 & 0 & -\overline{h}_{32} \\ 0 & 0 & \overline{c}_{44}^D & 0 & 0 & 0 \\ 0 & 0 & 0 & \overline{c}_{55}^D & 0 & -\overline{h}_{35} \\ 0 & 0 & 0 & 0 & \overline{c}_{66}^D & 0 \\ -\overline{h}_{31} & -\overline{h}_{32} & 0 & -\overline{h}_{35} & 0 & \overline{\beta}_{33}^\varepsilon \end{bmatrix} \begin{Bmatrix} \varepsilon_1 \\ \varepsilon_2 \\ \varepsilon_4 \\ \varepsilon_5 \\ \varepsilon_6 \\ D_3 \end{Bmatrix}. \tag{6}$$

In this work, two polarization schemes were considered. Each piezoelectric layer may be poled in x- or z-direction. In the first case, the piezoelectric layer responds to transverse shear strains, ε_5, while in the second case, it responds to normal strains, ε_1 and ε_2. The constitutive equations for a piezoelectric material poled in the x-direction may be obtained from the standard z-poled ones through a 90° rotation around the y-direction [24]. In order to use a unified constitutive equation (6) for both cases using the properties for a z-poled piezoelectric material provided by the manufacturers, the modified elastic, piezoelectric and dielectric constants are defined as

$$\overline{c}_{11}^D = (c_{11}^D - {c_{13}^D}^2/c_{33}^D), \quad \overline{c}_{22}^D = (c_{22}^D - {c_{23}^D}^2/c_{33}^D),$$

$$\overline{c}_{12}^D = (c_{12}^D - c_{13}^D c_{23}^D/c_{33}^D), \quad \overline{c}_{44}^D = c_{44}^D, \quad \overline{c}_{55}^D = c_{55}^D, \quad \overline{c}_{66}^D = c_{66}^D,$$

$$\overline{\beta}_{33}^\varepsilon = (\beta_{33}^\varepsilon - h_{33}^2/c_{33}^D), \quad \overline{h}_{35} = 0,$$

$$\overline{h}_{31} = (h_{31} - h_{33}c_{13}^D/c_{33}^D), \quad \overline{h}_{32} = (h_{32} - h_{33}c_{23}^D/c_{33}^D), \tag{7}$$

for piezoelectric layers poled in the z-direction and

$$\overline{c}^D_{11} = (c^D_{33} - {c^D_{13}}^2/c^D_{11}), \quad \overline{c}^D_{22} = (c^D_{22} - {c^D_{12}}^2/c^D_{11}),$$

$$\overline{c}^D_{12} = (c^D_{23} - c^D_{12}c^D_{13}/c^D_{11}), \quad \overline{c}^D_{44} = c^D_{66}, \quad \overline{c}^D_{55} = c^D_{55}, \quad \overline{c}^D_{66} = c^D_{44},$$

$$\overline{\beta}^{\varepsilon}_{33} = \beta^{\varepsilon}_{11}, \quad \overline{h}_{35} = h_{15},$$

$$\overline{h}_{31} = \overline{h}_{32} = 0, \tag{8}$$

for those poled in the x-direction. From (6) to (8), it is possible to observe that the electromechanical coupling is between through-thickness electric field, or displacement, and normal strains ε_1 and ε_2, for a piezoelectric layer poled in the z-direction, or transverse shear strains ε_5, for a piezoelectric layer poled in the x-direction.

2.3. Variational formulation

The equations of motion for the laminate plate composed of elastic and piezoelectric (z-poled or x-poled) layers are obtained using Hamilton's principle

$$\int_t (\delta T - \delta U + \delta W)\,\mathrm{d}t = 0, \tag{9}$$

such that the virtual variation of electromechanical potential energy δU of the laminate plate may be written from (4) as

$$\delta U(\boldsymbol{\varepsilon},\mathbf{D}) = \delta U_m - \delta U_{me} - \delta U_{em} + \delta U_e, \tag{10}$$

with

$$\delta U_m = \int_\Omega \delta\boldsymbol{\varepsilon}^{\mathrm{t}}\overline{\mathbf{c}}^D\boldsymbol{\varepsilon}\,\mathrm{d}\Omega, \quad \delta U_{me} = \int_\Omega \delta\boldsymbol{\varepsilon}^{\mathrm{t}}\overline{\mathbf{h}}^{\mathrm{t}}\mathbf{D}\,\mathrm{d}\Omega,$$

$$\delta U_{em} = \int_\Omega \delta\mathbf{D}^{\mathrm{t}}\overline{\mathbf{h}}\boldsymbol{\varepsilon}\,\mathrm{d}\Omega, \quad \delta U_e = \int_\Omega \delta\mathbf{D}^{\mathrm{t}}\overline{\boldsymbol{\beta}}^{\varepsilon}\mathbf{D}\,\mathrm{d}\Omega. \tag{11}$$

The virtual variation of kinetic energy δT is written in terms of the mechanical displacements u, v and w such that

$$\int_t \delta T\,\mathrm{d}t = -\int_t\int_\Omega \rho(\delta u\ddot{u} + \delta v\ddot{v} + \delta w\ddot{w})\,\mathrm{d}\Omega\,\mathrm{d}t, \tag{12}$$

where $\ddot{u}$, $\ddot{v}$ and $\ddot{w}$ represent the accelerations in the directions x, y and z, respectively. The virtual work done by the external mechanical forces δW is defined a posteriori in the finite element model.

2.4. Finite element discretization

With the objective of obtaining a discrete finite element model for the laminate plate, for which a single mechanical displacements field is considered for all layers while electric displacements in each layer are independent, this section presents the finite element discretization of mechanical and electric displacements.

A rectangular finite element model with four nodes is considered using linear Lagrange's interpolation functions for the in-plane displacements, u_0 and v_0, and cross-section rotations at midplane, ψ_x and ψ_y, and cubic Hermite's interpolation functions, nonconforming, for the transversal displacement w_0. For the electric displacements in each layer, linear Lagrange's interpolation functions were also considered. Therefore, a four-node finite element model with seven mechanical degrees of freedom, u_0, v_0, ψ_x, ψ_y, w_0, $w_{0,x}$ and $w_{0,y}$, and four (per piezoelectric layer) electrical degrees of freedom is obtained.

2.4.1. Discretization of mechanical displacements and strains

Using the considerations described above, the generalized mechanical displacements u_0, v_0, ψ_x, ψ_y and w_0 can be written as

$$u_0(x,y,t) = \sum_{j=1}^{4} u_0^j(t)N_j(x,y), \quad v_0(x,y,t) = \sum_{j=1}^{4} v_0^j(t)N_j(x,y),$$

$$\psi_x(x,y,t) = \sum_{j=1}^{4} \psi_x^j(t)N_j(x,y), \quad \psi_y(x,y,t) = \sum_{j=1}^{4} \psi_y^j(t)N_j(x,y),$$

$$w_0(x,y,t) = \sum_{j=1}^{4} [w_0^j(t)N_5^j(x,y) + w_{0,x}^j(t)N_6^j(x,y) + w_{0,y}^j(t)N_7^j(x,y)], \tag{13}$$

where the interpolation functions $N_j(x,y)$, $N_5^j(x,y)$, $N_6^j(x,y)$ and $N_7^j(x,y)$ ($j=1,\ldots,4$) are defined as

$$\begin{Bmatrix} N_1 \\ N_2 \\ N_3 \\ N_4 \end{Bmatrix} = \frac{1}{4}\begin{bmatrix} (1-\xi)(1-\eta) \\ (1+\xi)(1-\eta) \\ (1+\xi)(1+\eta) \\ (1-\xi)(1+\eta) \end{bmatrix}, \tag{14}$$

$$\begin{Bmatrix} N_5^j \\ N_6^j \\ N_7^j \end{Bmatrix} = \frac{1}{8}\begin{bmatrix} (1+\xi_0)(1+\eta_0)(2+\xi_0+\eta_0-\xi^2-\eta^2) \\ \xi_j(\xi_0-1)(1+\eta_0)(1+\xi_0)^2 \\ \eta_j(\eta_0-1)(1+\xi_0)(1+\eta_0)^2 \end{bmatrix}. \tag{15}$$

The natural coordinates are defined as $\xi=(x/a)$, $\eta=(y/b)$, $\xi_0=\xi\xi_j$ and $\eta_0=\eta\eta_j$, with $\xi_j=(x_j/a)$ and $\eta_j=(y_j/b)$, where x_j and y_j correspond to the node position on the element, that is, $x_j=a$ or $x_j=-a$ and $y_j=b$ or $y_j=-b$. a and b are the half-dimension of the element along the directions x and y, respectively, as shown in Fig. 2.

The generalized displacements u_0, v_0, w_0, ψ_x and ψ_y can be grouped in a vector $\mathbf{u}_g$ such that

$$\mathbf{u}_g=[u_0 \;\; v_0 \;\; w_0 \;\; \psi_x \;\; \psi_y]^{\mathrm{t}} \tag{16}$$

Then, the vector of generalized displacements $\mathbf{u}_g$ can be written as a function of the nodal displacements vector $\mathbf{u}_e$ as

$$\mathbf{u}_g=\mathbf{N}_g\mathbf{u}_e, \tag{17}$$

with

$$\mathbf{u}_e=[\mathbf{u}_e^1 \;\; \mathbf{u}_e^2 \;\; \mathbf{u}_e^3 \;\; \mathbf{u}_e^4]^{\mathrm{t}}, \tag{18}$$

$$\mathbf{u}_e^j=[u_0^j \;\; v_0^j \;\; w_0^j \;\; w_{0,x}^j \;\; w_{0,y}^j \;\; \psi_x^j \;\; \psi_y^j]^{\mathrm{t}}, \quad \mathrm{j}=1,\ldots,4. \tag{19}$$

The interpolation matrix for $\mathbf{u}_g$ can then be written as

$$\mathbf{N}_g=[\mathbf{N}_g^1 \;\; \mathbf{N}_g^2 \;\; \mathbf{N}_g^3 \;\; \mathbf{N}_g^4],$$

$$\mathbf{N}_g^j=\begin{bmatrix} N_j & 0 & 0 & 0 & 0 & 0 & 0 \\ 0 & N_j & 0 & 0 & 0 & 0 & 0 \\ 0 & 0 & N_5^j & N_6^j & N_7^j & 0 & 0 \\ 0 & 0 & 0 & 0 & 0 & N_j & 0 \\ 0 & 0 & 0 & 0 & 0 & 0 & N_j \end{bmatrix}. \tag{20}$$

The generalized strains defined in (2) can also be grouped in a vector $\boldsymbol{\varepsilon}_g$, such that,

$$\boldsymbol{\varepsilon}_g=[\varepsilon_1^0 \;\; \varepsilon_2^0 \;\; \varepsilon_4^0 \;\; \varepsilon_5^0 \;\; \varepsilon_6^0 \;\; \varepsilon_1^1 \;\; \varepsilon_2^1 \;\; \varepsilon_6^1 \;\; \varepsilon_4^2 \;\; \varepsilon_5^2 \;\; \varepsilon_1^3 \;\; \varepsilon_2^3 \;\; \varepsilon_6^3]^{\mathrm{t}}, \tag{21}$$

and written as a function of the generalized displacements vector in the form

$$\boldsymbol{\varepsilon}_g=\mathbf{L}_\varepsilon\mathbf{u}_g, \tag{22}$$

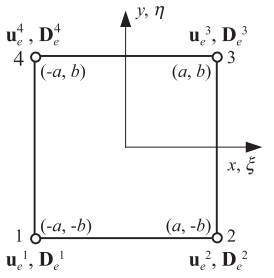

Fig. 2. Schematic representation of the laminate plate finite element.

with

$$\mathbf{L}_\varepsilon = \begin{bmatrix} \frac{\partial}{\partial x} & 0 & 0 & 0 & 0 \\ 0 & \frac{\partial}{\partial y} & 0 & 0 & 0 \\ 0 & 0 & \frac{\partial}{\partial y} & 0 & 1 \\ 0 & 0 & \frac{\partial}{\partial x} & 1 & 0 \\ \frac{\partial}{\partial y} & \frac{\partial}{\partial x} & 0 & 0 & 0 \\ 0 & 0 & 0 & \frac{\partial}{\partial x} & 0 \\ 0 & 0 & 0 & 0 & \frac{\partial}{\partial y} \\ 0 & 0 & 0 & \frac{\partial}{\partial y} & \frac{\partial}{\partial x} \\ 0 & 0 & \frac{\partial}{\partial y} & 0 & 1 \\ 0 & 0 & \frac{\partial}{\partial x} & 1 & 0 \\ 0 & 0 & \frac{\partial^2}{\partial x^2} & \frac{\partial}{\partial x} & 0 \\ 0 & 0 & \frac{\partial^2}{\partial y^2} & 0 & \frac{\partial}{\partial y} \\ 0 & 0 & 2\frac{\partial^2}{\partial x \partial y} & \frac{\partial}{\partial y} & \frac{\partial}{\partial x} \end{bmatrix}. \tag{23}$$

Finally, using (17) and (22), the generalized strains can be written as a function of the nodal displacements as

$$\varepsilon_g = \mathbf{B}\mathbf{u}_e \quad \text{where } \mathbf{B} = \mathbf{L}_\varepsilon \mathbf{N}_g \text{ or } \varepsilon_i^j = \mathbf{B}_{ij}\mathbf{u}_e. \tag{24}$$

2.4.2. Discretization of electric displacements

The through-thickness electric displacements in the $2n$ layers can be grouped as a vector $\mathbf{D}_d$

$$\mathbf{D}_d = [D_3^{(n)}(x,y,t)\ \ D_3^{(n-1)}(x,y,t)\ \ \cdots\ \ D_3^{-(n-1)}(x,y,t)\ \ D_3^{(-n)}(x,y,t)]^{\mathrm{t}}, \tag{25}$$

and written as a function of the nodal electric displacements in the form

$$\mathbf{D}_d = \mathbf{N}_D \mathbf{D}_e, \tag{26}$$

where

$$\mathbf{D}_e = [\mathbf{D}_e^1\ \ \mathbf{D}_e^2\ \ \mathbf{D}_e^3\ \ \mathbf{D}_e^4]^{\mathrm{t}},$$

$$\mathbf{D}_e^j = [D_3^{(n),j}\ \ D_3^{(n-1),j}\ \ \cdots\ \ D_3^{-(n-1),j}\ \ D_3^{(-n),j}]^{\mathrm{t}}. \tag{27}$$

Considering linear Lagrange's interpolation functions for electric displacements, the interpolation matrix N_D is written as

$$\mathbf{N}_D = [\mathbf{N}_1\ \ \mathbf{N}_2\ \ \mathbf{N}_3\ \ \mathbf{N}_4], \quad \mathbf{N}_j = \mathrm{diag}(N_j). \tag{28}$$

Notice that the dimension of $\mathbf{N}_j$ is $(2n \times 2n)$ and, therefore, that of $\mathbf{N}_D$ is $[2n \times (2n \times 4)]$.

2.4.3. Discretization of energy virtual variations

Using the discretization of mechanical displacements and strains and electric displacements previously presented, it is possible to discretize the virtual variations of potential (11) and kinetic (12) energies. Replacing (24) and (26) in (11), one gets

$$\delta U_m = \delta \mathbf{u}_e^{\mathrm{t}} \mathbf{K}_m^e \mathbf{u}_e, \quad \delta U_{me} = \delta \mathbf{u}_e^{\mathrm{t}} \mathbf{K}_{me}^e \mathbf{D}_e,$$

$$\delta U_{em} = \delta \mathbf{D}_e^{\mathrm{t}} \mathbf{K}_{me}^{e\ \mathrm{t}} \mathbf{u}_e, \quad \delta U_e = \delta \mathbf{D}_e^{\mathrm{t}} \mathbf{K}_e^e \mathbf{D}_e, \tag{29}$$

where the elastic $\mathbf{K}_m^e$, piezoelectric $\mathbf{K}_{me}^e$ and dielectric $\mathbf{K}_e^e$ elementary stiffness matrices are evaluated from

$$\mathbf{K}_m^e = 2\sum_{i=1}^{n} \int_{-b}^{b} \int_{-a}^{a} \left\{ (z_i - z_{i-1}) \left[\sum_{k=1,2,4,5,6} \overline{c}_{kk}^{Di} (\mathbf{B}_{k0}^{\mathrm{t}} \mathbf{B}_{k0}) + \overline{c}_{12}^{Di} (\mathbf{B}_{20}^{\mathrm{t}} \mathbf{B}_{10} + \mathbf{B}_{10}^{\mathrm{t}} \mathbf{B}_{20}) \right] \right.$$

$$+\frac{(z_i^3-z_{i-1}^3)}{3}\left[\sum_{k=1,2,6}\overline{c}_{kk}^{Di}(\mathbf{B}_{k1}^{\mathrm{t}}\mathbf{B}_{k1})-3c_1\sum_{k=4,5}\overline{c}_{kk}^{Di}(\mathbf{B}_{k0}^{\mathrm{t}}\mathbf{B}_{k2}+\mathbf{B}_{k2}^{\mathrm{t}}\mathbf{B}_{k0})\right]$$
$$-\frac{c_1}{5}(z_i^5-z_{i-1}^5)\left[\sum_{k=1,2,6}\overline{c}_{kk}^{Di}(\mathbf{B}_{k1}^{\mathrm{t}}\mathbf{B}_{k3}+\mathbf{B}_{k3}^{\mathrm{t}}\mathbf{B}_{k1})-9c_1\sum_{k=4,5}\overline{c}_{kk}^{Di}\mathbf{B}_{k2}^{\mathrm{t}}\mathbf{B}_{k2}+\overline{c}_{12}^{Di}(\mathbf{B}_{21}^{\mathrm{t}}\mathbf{B}_{13}+\mathbf{B}_{13}^{\mathrm{t}}\mathbf{B}_{21}+\mathbf{B}_{11}^{\mathrm{t}}\mathbf{B}_{23}+\mathbf{B}_{23}^{\mathrm{t}}\mathbf{B}_{11})\right]$$
$$+\frac{c_1^2}{7}(z_i^7-z_{i-1}^7)\left[\sum_{k=1,2,6}\overline{c}_{kk}^{Di}(\mathbf{B}_{k3}^{t}\mathbf{B}_{k3})+\overline{c}_{12}^{Di}(\mathbf{B}_{13}^{\mathrm{t}}\mathbf{B}_{23}+\mathbf{B}_{23}^{\mathrm{t}}\mathbf{B}_{13})\right]\Bigg\}\mathrm{d}x\,\mathrm{d}y, \tag{30}$$

$$\mathbf{K}_{me}^{e}=\sum_{i=1}^{n}\int_{-b}^{b}\int_{-a}^{a}\Bigg\{(z_i-z_{i-1})[\overline{h}_{31}^{i}\mathbf{B}_{10}^{\mathrm{t}}+\overline{h}_{32}^{i}\mathbf{B}_{20}^{\mathrm{t}}+\overline{h}_{35}^{i}\mathbf{B}_{50}^{\mathrm{t}}](\mathbf{N}_D^i+\mathbf{N}_D^{-i})+\frac{1}{2}(z_i^2-z_{i-1}^2)[\overline{h}_{31}^{i}\mathbf{B}_{11}^{\mathrm{t}}+\overline{h}_{32}^{i}\mathbf{B}_{21}^{\mathrm{t}}](\mathbf{N}_D^i-\mathbf{N}_D^{-i})$$
$$-c_1(z_i^3-z_{i-1}^3)[\overline{h}_{35}^{i}\mathbf{B}_{52}^{\mathrm{t}}](\mathbf{N}_D^i+\mathbf{N}_D^{-i})-\frac{c_1}{4}(z_i^4-z_{i-1}^4)[\overline{h}_{31}^{i}\mathbf{B}_{13}^{\mathrm{t}}+\overline{h}_{32}^{i}\mathbf{B}_{23}^{\mathrm{t}}](\mathbf{N}_D^i-\mathbf{N}_D^{-i})\Bigg\}\mathrm{d}x\,\mathrm{d}y, \tag{31}$$

$$\mathbf{K}_{e}^{e}=2\sum_{i=1}^{n}\int_{-b}^{b}\int_{-a}^{a}(z_i-z_{i-1})\overline{\beta}_{33}^{i}(\mathbf{N}_D^i)^{\mathrm{t}}\mathbf{N}_D^i\,\mathrm{d}x\,\mathrm{d}y. \tag{32}$$

The virtual variation of kinetic energy and virtual work of external mechanical forces are

$$\int_t\delta T\,\mathrm{d}t=-\int_t\delta\mathbf{u}_e^{\mathrm{t}}\mathbf{M}^e\ddot{\mathbf{u}}_e\,\mathrm{d}t, \tag{33}$$

$$\delta W=\delta\mathbf{u}_e^{\mathrm{t}}\mathbf{F}_m^e, \tag{34}$$

where the vector of elementary external mechanical forces $\mathbf{F}_m^e$ is defined for the global nodes after assembly and the elementary mass matrix $\mathbf{M}^e$ is written, using (1), (12) and (17), as

$$\mathbf{M}^e=2\sum_{i=1}^{n}\int_{-b}^{b}\int_{-a}^{a}\rho^i\Bigg\{(z_i-z_{i-1})[\mathbf{N}_u^{\mathrm{t}}\mathbf{N}_u+\mathbf{N}_v^{\mathrm{t}}\mathbf{N}_v+\mathbf{N}_w^{\mathrm{t}}\mathbf{N}_w]+\frac{1}{3}(z_i^3-z_{i-1}^3)[\mathbf{N}_{\psi_x}^{\mathrm{t}}\mathbf{N}_{\psi_x}+\mathbf{N}_{\psi_y}^{\mathrm{t}}\mathbf{N}_{\psi_y}]-\frac{c_1}{5}(z_i^5-z_{i-1}^5)$$
$$\times[2\mathbf{N}_{\psi_x}^{\mathrm{t}}\mathbf{N}_{\psi_x}+\mathbf{N}_{\psi_x}^{\mathrm{t}}\mathbf{N}_{w,x}+\mathbf{N}_{w,x}^{\mathrm{t}}\mathbf{N}_{\psi_x}+2\mathbf{N}_{\psi_y}^{\mathrm{t}}\mathbf{N}_{\psi_y}+\mathbf{N}_{\psi_y}^{\mathrm{t}}\mathbf{N}_{w,y}+\mathbf{N}_{w,y}^{\mathrm{t}}\mathbf{N}_{\psi_y}]+\frac{c_1^2}{7}(z_i^7-z_{i-1}^7)$$
$$\times[\mathbf{N}_{\psi_x}^{\mathrm{t}}\mathbf{N}_{\psi_x}+\mathbf{N}_{\psi_x}^{\mathrm{t}}\mathbf{N}_{w,x}+\mathbf{N}_{w,x}^{\mathrm{t}}\mathbf{N}_{\psi_x}+\mathbf{N}_{w,x}^{\mathrm{t}}\mathbf{N}_{w,x}+\mathbf{N}_{\psi_y}^{\mathrm{t}}\mathbf{N}_{\psi_y}+\mathbf{N}_{\psi_y}^{\mathrm{t}}\mathbf{N}_{w,y}+\mathbf{N}_{w,y}^{\mathrm{t}}\mathbf{N}_{\psi_y}+\mathbf{N}_{w,y}^{\mathrm{t}}\mathbf{N}_{w,y}]\Bigg\}\mathrm{d}x\,\mathrm{d}y. \tag{35}$$

2.5. Coupled equations of motion

Replacing the discretized form of the elementary virtual variations of potential (29) and kinetic (33) energies and virtual work of external mechanical forces (34) into Hamilton's principle and, then, assembling the equations for all finite elements yields the following global equations of motion, written in terms of the nodal mechanical and electrical degrees of freedom,

$$\begin{bmatrix}\mathbf{M}&0\\0&0\end{bmatrix}\begin{Bmatrix}\ddot{\mathbf{u}}\\\ddot{\mathbf{D}}\end{Bmatrix}+\begin{bmatrix}\mathbf{K}_m&-\mathbf{K}_{me}\\-\mathbf{K}_{me}^{\mathrm{t}}&\mathbf{K}_e\end{bmatrix}\begin{Bmatrix}\mathbf{u}\\\mathbf{D}\end{Bmatrix}=\begin{Bmatrix}\mathbf{F}_m\\0\end{Bmatrix}, \tag{36}$$

where $\mathbf{M}$, $\mathbf{K}_m$, $\mathbf{K}_{me}$ and $\mathbf{K}_e$ are mass and elastic, piezoelectric and dielectric stiffness global matrices, respectively. $\mathbf{u}$ and $\mathbf{D}$ are the global vectors of nodal mechanical and electrical degrees of freedom. More details in this formulation can be found in [25].

These equations of motion account for the coupling between mechanical displacements of whole laminate plate, including piezoelectric layers, and electric displacements induced in the piezoelectric layers. It is possible to consider different boundary conditions for both mechanical and electrical quantities, for instance open ($\mathbf{D}=0$) and closed ($\mathbf{D}\neq0$) circuit conditions for the piezoelectric layers. However, in this work, it is supposed that each piezoelectric layer may be connected to an electric circuit, composed of resistance, inductance and voltage source. For a series of independent resonant (resistive–inductive) electric circuits coupled to voltage sources, the equations of motion are

$$\mathbf{L}_c\ddot{\mathbf{q}}_c+\mathbf{R}_c\dot{\mathbf{q}}_c=\mathbf{V}_c, \tag{37}$$

where $\mathbf{L}_c$ and $\mathbf{R}_c$ are diagonal matrices and $\mathbf{q}_c$ and $\mathbf{V}_c$ are vectors with elements L_c^j, R_c^j, q_c^j and V_c^j, respectively, which are the inductance, resistance, electric charge and applied voltage for the j-th circuit.

Combining the equations of motion of the circuits with those of the structure with piezoelectric elements yields

$$\begin{bmatrix}\mathbf{M}&0&0\\0&0&0\\0&0&\mathbf{L}_c\end{bmatrix}\begin{Bmatrix}\ddot{\mathbf{u}}\\\ddot{\mathbf{D}}\\\ddot{\mathbf{q}}_c\end{Bmatrix}+\begin{bmatrix}0&0&0\\0&0&0\\0&0&\mathbf{R}_c\end{bmatrix}\begin{Bmatrix}\dot{\mathbf{u}}\\\dot{\mathbf{D}}\\\dot{\mathbf{q}}_c\end{Bmatrix}+\begin{bmatrix}\mathbf{K}_m&-\mathbf{K}_{me}&0\\-\mathbf{K}_{me}^{\mathrm{t}}&\mathbf{K}_e&0\\0&0&0\end{bmatrix}\begin{Bmatrix}\mathbf{u}\\\mathbf{D}\\\mathbf{q}_c\end{Bmatrix}=\begin{Bmatrix}\mathbf{F}_m\\0\\\mathbf{V}_c\end{Bmatrix}. \tag{38}$$

In order to couple the electric circuits and piezoelectric structure, two additional steps should be undertaken. First, an equipotential surface representing the electrodes over the upper and lower surfaces of the piezoelectric layers must be reinforced. This is done by rewriting the global vector of nodal electric displacements $\mathbf{D}$ in terms of a vector of electric displacements in each independent piezoelectric patch or layer, such that

$$\mathbf{D} = \mathbf{L}_p \mathbf{D}_p, \quad \mathbf{D}_p = [D_{p1} \;\; D_{p2} \;\; D_{p3} \;\; \cdots \;\; D_{pm}]^{\mathrm{t}}, \tag{39}$$

where $\mathbf{L}_p$ is a binary matrix that imposes the equality between the electric displacements at the nodes located in the region covered by an electrode. Then, the total electric charge accumulated in an electrode is related to the electric displacement by $\mathbf{q}_p = \mathbf{A}_p \mathbf{D}_p$, where $\mathbf{A}_p$ is a diagonal matrix containing the surface area of the electrodes covering each piezoelectric patch. Next, it is assumed that all electric charge accumulated in an electrode will flow through the circuit to which it is connected. This allows to write an equality relation between the electric charge $\mathbf{q}_p$, and thus the electric displacement $\mathbf{D}_p$, in the patches and the electric charge $\mathbf{q}_c$ in the circuits, such that $\mathbf{D}_p = \mathbf{A}_p^{-1}\mathbf{q}_p = \mathbf{A}_p^{-1}\mathbf{q}_c$. Replacing this relation into (39) leads to

$$\mathbf{D} = \mathbf{B}_p \mathbf{q}_c, \quad \mathbf{B}_p = \mathbf{L}_p \mathbf{A}_p^{-1}. \tag{40}$$

Replacing (40) in a variational form of the equations of motion (38) and summing the terms related to $\mathbf{q}_c$, one gets the following reduced equations of motion in terms of the mechanical displacements $\mathbf{u}$ and circuits' electric charges $\mathbf{q}_c$

$$\begin{bmatrix} \mathbf{M} & 0 \\ 0 & \mathbf{L}_c \end{bmatrix} \begin{Bmatrix} \ddot{\mathbf{u}} \\ \ddot{\mathbf{q}}_c \end{Bmatrix} + \begin{bmatrix} 0 & 0 \\ 0 & \mathbf{R}_c \end{bmatrix} \begin{Bmatrix} \dot{\mathbf{u}} \\ \dot{\mathbf{q}}_c \end{Bmatrix} + \begin{bmatrix} \mathbf{K}_m & -\overline{\mathbf{K}}_{me} \\ -\overline{\mathbf{K}}_{me}^{\mathrm{t}} & \overline{\mathbf{K}}_e \end{bmatrix} \begin{Bmatrix} \mathbf{u} \\ \mathbf{q}_c \end{Bmatrix} = \begin{Bmatrix} \mathbf{F}_m \\ \mathbf{V}_c \end{Bmatrix}, \tag{41}$$

where $\overline{\mathbf{K}}_{me} = \mathbf{K}_{me}\mathbf{B}_p$ and $\overline{\mathbf{K}}_e = \mathbf{B}_p^{\mathrm{t}}\mathbf{K}_e\mathbf{B}_p$.

3. Finite element model validation

The proposed finite element model was implemented in Matlab. In this section, eigenfrequency results obtained with the proposed model are compared to numerical and analytical results found in the open literature, considering only open and closed circuit boundary conditions for the piezoelectric layers, that is without connection to an electric circuit.

3.1. Laminate plate with through-thickness poled piezoelectric layers

In this case, a square laminate plate composed of three layers of Graphite-Epoxy (GE, Carbon-Fibre Reinforced) material (0/90/0) covered by PZT-4 piezoelectric layers poled in z-direction (through-thickness) is considered, leading to a five-layer laminate plate (PZT-4/GE 0°/GE 90°/GE 0°/PZT-4). The thickness of piezoelectric and GE layers are 1 and 2.67 mm, respectively, and plate's length is 500 mm. The material properties of PZT-4 poled in z-direction are [26]: $c_{11}^E = c_{22}^E = 138.5$ GPa, $c_{33}^E = 114.75$ GPa, $c_{12}^E = 77.37$ GPa, $c_{13}^E = c_{23}^E = 73.64$ GPa, $c_{44}^E = c_{55}^E = 25.60$ GPa, $c_{66}^E = 30.60$ GPa, $e_{15} = e_{24} = 12.72\,\mathrm{C\,m^{-2}}$, $e_{31} = e_{32} = -5.2\,\mathrm{C\,m^{-2}}$, $e_{33} = 15.08\,\mathrm{C\,m^{-2}}$, $\varepsilon_{11}^\sigma = \varepsilon_{22}^\sigma = 15.3\,\mathrm{nF\,m^{-1}}$, $\varepsilon_{33}^\sigma = 15\,\mathrm{nF\,m^{-1}}$. The material properties of the GE (0°) are [26]: $c_{11} = 133$ GPa, $c_{22} = 10.81$ GPa, $c_{33} = 14.36$ GPa, $c_{12} = 2.59$ GPa, $c_{13} = 5.16$ GPa, $c_{23} = 7.14$ GPa, $c_{44} = 3.61$ GPa, $c_{55} = c_{66} = 5.65$ GPa. The densities of all materials were considered to be unitary, $1\,\mathrm{kg\,m^{-3}}$, for comparisons purpose. The plate was considered to be simply supported (SSSS). Four hundred plate elements were used in this analysis.

The first five natural frequencies $\omega_{x,y}$ were evaluated and re-dimensionalized by the expression $\lambda_{x,y} = \omega_{x,y} L^2 \sqrt{\rho}/2\pi h$. The results obtained by FSDT and TSDT models were compared to the analytical solutions 3D-SSM (State Space Method, coupled) by Benjeddou and Deü [21] and finite element solutions Q9-HSDT (Higher Shear Deformation Theory, with nine nodes per element and 11 degrees of freedom) by Franco Correia et al. [26], in short-circuit (SC) and open-circuit (OC). The present results and their percent errors relative to the published ones ($\Delta\%$) are shown in Table 1. It is possible to observe that a reasonably good approximation to 3D-SSM and Q9-HSDT theories is obtained, although the relative error for some eigenfrequencies are greater than 5%. For this plate configuration, the present FSDT model yields higher eigenfrequencies

Table 1
First five eigenfrequencies of laminate plate PZT-4/GE 0°/GE 90°/GE 0°/PZT-4.

	SC					OC				
	$\lambda_{1,1}$	$\lambda_{1,2}$	$\lambda_{2,1}$	$\lambda_{2,2}$	$\lambda_{1,3}$	$\lambda_{1,1}$	$\lambda_{1,2}$	$\lambda_{2,1}$	$\lambda_{2,2}$	$\lambda_{1,3}$
3D	245.94	559.40	691.73	965.18	1090.98	245.94	559.41	691.73	965.19	1091.00
Q9	230.46	520.38	662.91	908.46	1022.09	250.50	583.18	695.70	980.36	1145.41
FSDT	227.65	547.81	690.55	921.65	1118.41	231.08	547.81	690.55	921.65	1120.37
$\Delta\%$(3D)	−8.03	−2.12	−0.17	−4.72	2.45	−6.43	−2.12	−0.17	−4.72	2.62
$\Delta\%$(Q9)	−1.23	5.01	4.00	1.43	8.61	−8.40	−6.46	−0.75	−6.37	−2.23
TSDT	225.98	542.29	680.11	906.09	1099.05	229.41	542.29	680.11	906.09	1100.94
$\Delta\%$(3D)	−8.83	−3.16	−1.71	−6.52	0.73	−7.20	−3.16	−1.71	−6.52	0.90
$\Delta\%$(Q9)	−1.98	4.04	2.53	−0.26	7.00	−9.19	−7.54	−2.29	−8.20	−4.04

than the TSDT one. Differences between eigenfrequencies for piezoelectric layers in SC and OC conditions occur only in symmetric modes for both models, FSDT and TSDT, which is reasonable since asymmetric modes leads to asymmetric distribution of electric potential on the electrodes of piezoelectric layers leading to a charge cancelation effect [29].

3.2. Sandwich plates with longitudinally poled piezoelectric layers

In a first analysis, a square sandwich plate with Graphite-Epoxy (GE, Carbon-Fibre Reinforced) surface layers and a longitudinally poled (x-direction) PZT-5H piezoelectric core layer is considered (GE 0°/PZT-5H/GE 0°). Plate dimensions are: total thickness $H=1$ cm and length $L=10$ cm, GE layers thicknesses 0.4 cm and PZT-5H layer thickness 0.2 cm. Material properties for a through-thickness poled PZT-5H are [15]: $c_{11}^E=c_{22}^E=126$ GPa, $c_{33}^E=117$ GPa, $c_{12}^E=79.5$ GPa, $c_{13}^E=c_{23}^E=84.1$ GPa, $c_{44}^E=c_{55}^E=c_{66}^E=23$ GPa, $e_{15}=e_{24}=17\,\mathrm{C\,m^{-2}}$, $e_{31}=e_{32}=-6.5\,\mathrm{C\,m^{-2}}$, $e_{33}=23.3\,\mathrm{C\,m^{-2}}$, $\varepsilon_{11}^{\varepsilon}=\varepsilon_{22}^{\varepsilon}=15.03\,\mathrm{nF\,m^{-1}}$, $\varepsilon_{33}^{\varepsilon}=13\,\mathrm{nF\,m^{-1}}$, $\rho^{pzt}=7500\,\mathrm{kg\,m^{-3}}$. GE material properties are [15]: $c_{11}=183.443$ GPa, $c_{22}=c_{33}=11.662$ GPa, $c_{12}=c_{13}=4.363$ GPa, $c_{23}=3.918$ GPa, $c_{44}=2.870$ GPa, $c_{55}=c_{66}=7.170$ GPa, $\rho^{GE}=1580\,\mathrm{kg\,m^{-3}}$. The plate is considered to be simply supported (SSSS). Nine hundred plate elements were used in this analysis.

The results obtained with the proposed models, based on FSDT and TSDT, were compared to analytical solutions 3D MSSA (Mixed State Space Approach) obtained by Deü and Benjeddou [15], in SC and OC conditions. Table 2 presents the first eight non-dimensional eigenfrequencies, $\lambda_{x,y}=\omega_{x,y}L^2\sqrt{(\rho^{pzt}/c_{55}^E pzt)}/H$, for the plate evaluated with the present models and their comparisons with the analytical results. It is possible to observe that the results of the present model are close to those obtained by Deü and Benjeddou [15], although for some eigenfrequencies the error is larger than 5%. TSDT is closer than FSDT to reference results for lower eigenfrequencies while, for higher eigenfrequencies, FSDT is closer to reference results. It was also observed that the TSDT model yields higher eigenfrequencies than the FSDT one. No difference between SC and OC conditions were found, which can be explained by the fact that all vibration modes yield an asymmetric shear strain distribution and, thus, leading to charge cancelation due to equipotentiality.

A second analysis was performed with a sandwich plate GE 0°/PZT-5A/GE 0° studied by Baillargeon and Vel [27]. The plate is considered to have infinite extent in y-direction. The thickness of GE and PZT-5A layers are considered to be 1 and 0.5 mm, respectively, leading to a total thickness of 2.5 mm, and the length along the finite direction (x) is $L=250$ mm. The plate is simply supported at the boundaries along the finite direction (SSFF). The material properties of through-thickness poled PZT-5A are [27]: $c_{11}^E=c_{22}^E=99.201$ GPa, $c_{33}^E=86.856$ GPa, $c_{12}^E=54.016$ GPa, $c_{13}^E=c_{23}^E=50.778$ GPa, $c_{44}^E=c_{55}^E=21.100$ GPa, $c_{66}^E=22.600$ GPa, $e_{15}=e_{24}=12.322\,\mathrm{C\,m^{-2}}$, $e_{31}=e_{32}=-7.209\,\mathrm{C\,m^{-2}}$, $e_{33}=15.118\,\mathrm{C\,m^{-2}}$, $\varepsilon_{11}^{\sigma}=\varepsilon_{22}^{\sigma}=15.3\,\mathrm{nF\,m^{-1}}$, $\varepsilon_{33}^{\sigma}=15\,\mathrm{nF\,m^{-1}}$, $\rho^{pzt}=7750\,\mathrm{kg\,m^{-3}}$. Material properties of the GE material at 0° are the same of the previous analysis. Three hundred plate finite elements were used.

Table 2
First eight non-dimensional eigenfrequencies of sandwich plate GE 0°/PZT-5H/GE 0°.

Modo	SC					OC				
	Ref.	FSDT	Error (%)	TSDT	Error (%)	Ref.	FSDT	Error (%)	TSDT	Error (%)
$\lambda_{1,1}$	13.49	13.09	−3.06	13.29	−1.52	13.56	13.09	−3.56	13.29	−2.02
$\lambda_{1,2}$	19.77	18.69	−5.80	18.90	−4.61	19.84	18.69	−6.17	18.90	−4.98
$\lambda_{1,3}$	31.73	31.50	−0.74	31.82	0.28	31.80	31.50	−0.95	31.82	0.07
$\lambda_{2,1}$	40.68	42.51	4.31	44.52	8.63	41.26	42.51	2.95	44.52	7.33
$\lambda_{2,2}$	44.44	44.91	1.04	46.91	5.26	45.02	44.91	−0.26	46.91	4.02
$\lambda_{1,4}$	47.81	49.83	4.05	50.45	5.23	47.88	49.83	3.91	50.45	5.09
$\lambda_{2,3}$	52.33	52.01	−0.60	53.96	3.03	52.89	52.01	−1.69	53.96	1.99
$\lambda_{2,4}$	64.57	65.16	0.91	67.15	3.84	65.10	65.16	0.10	67.15	3.06

Table 3
First eight eigenfrequencies (Hz) of sandwich plate GE 0°/PZT-5A/GE 0°.

	SC					OC				
	Ref.	FSDT	Δ (%)	TSDT	Δ (%)	Ref.	FSDT	Δ (%)	TSDT	Δ (%)
$f_{1,1}$	145.06	145.19	0.09	145.13	0.05	145.06	145.19	0.09	145.13	0.05
$f_{2,1}$	578.54	579.85	0.23	579.60	0.18	578.65	579.85	0.21	579.60	0.16
$f_{3,1}$	1295.49	1301.22	0.44	1300.66	0.40	1296.04	1301.22	0.40	1300.66	0.36
$f_{4,1}$	2287.84	2304.78	0.74	2303.81	0.69	2289.53	2304.78	0.66	2303.81	0.62
$f_{5,1}$	3544.82	3584.38	1.10	3582.89	1.06	3548.85	3584.38	0.99	3582.89	0.95
$f_{6,1}$	5053.35	5132.34	1.54	5130.25	1.50	5061.46	5132.34	1.38	5130.25	1.34
$f_{7,1}$	6798.55	6939.68	2.03	6936.95	2.00	6813.07	6939.68	1.82	6936.95	1.79
$f_{8,1}$	8764.26	8996.26	2.58	8992.87	2.54	8788.09	8996.26	2.31	8992.87	2.28

Similarly to the previous study, the first eight eigenfrequencies, in SC and OC, were evaluated using the FSDT and TSDT models and compared to the analytical results published by Baillargeon and Vel [27]. The eigenfrequency results and their error relative to the reference analytical results (Δ) are presented in Table 3. One can notice a satisfactory concordance between the proposed models results and the reference ones. For the same reason of the previous analysis, no difference in eigenfrequency values was observed between SC and OC conditions.

4. Passive vibration control using resonant circuits

In this section, the previously presented TSDT finite element model is used to evaluate and optimize the performance of a passive vibration control system using piezoelectric patches connected to resonant (resistive–inductive) shunt circuits. This is done by first placing four pairs of piezoelectric patches in a laminate composite plate, so that the energy conversion between the plate and the electric circuits is maximized, and then designing the shunt circuit components (resistance and inductance) so that the reduction of vibration amplitude of the plate near the first four resonances is maximized. The plate is made of 12 Graphite-Epoxy (Carbon-Fibre Reinforced) AS4/3501-6 layers (90°/ 90°/ 0°/ 0°/ 90°/ 90°// 90°/ 90°/ 0°/ 0°/ 90°/ 90°), has dimensions ($250 \times 350 \times 1.5$) mm and is supposed to be clamped on all sides (CCCC). The piezoelectric patches are made of thickness-poled PZT-5A piezoceramic material with dimensions ($25 \times 25 \times 0.25$) mm. The material properties were adapted from [28] and, for the GE, are: c_{11}=146 GPa, c_{22}=9.71 GPa, c_{33}=11.7 GPa, c_{12}=2.91 GPa, c_{13}=4.92 GPa, c_{23}=4.76 GPa, c_{44}=3.45 GPa, c_{55}=c_{66}=4.14 GPa, $\rho^{GE} = 1389\,\mathrm{kg\,m^{-3}}$. The material properties of PZT-5A are the same as those presented previously.

4.1. Optimal positioning of piezoelectric patches on the plate

It is known that the squared modal electromechanical coupling coefficient (EMCC) is an adequate indicator of the amount of strain energy converted to electrical energy by a piezoelectric patch when the structure to which it is bonded/embedded vibrates in a given mode shape [29]. Therefore, the EMCC is used here as a metric to perform the positioning of four symmetric pairs of patches throughout the plate, via parametric analysis, such that each patch maximizes the EMCC of one of the first four vibration modes of the laminate plate.

In order to analyze the optimal positioning of piezoelectric patches that maximizes the electromechanical coupling, a parametric analysis was performed. This was done through variation of the x, y and z position of one symmetrical pair of patches and subsequent evaluation of the electromechanical coupling of the pair for the first four vibration modes. Three positions across the thickness z-direction were chosen based on a previous analysis. In the first two positions, each piezoelectric patch replaces part of the first and last two adjacent layers of graphite-epoxy, starting from the midplane, respectively. In the third case, the piezoelectric patches are bonded on the external (upper/lower) surfaces of the laminate plate. In the plane xy, nine positions in x and in y are considered according to Fig. 3. Seven hundred plate elements were used in this analysis.

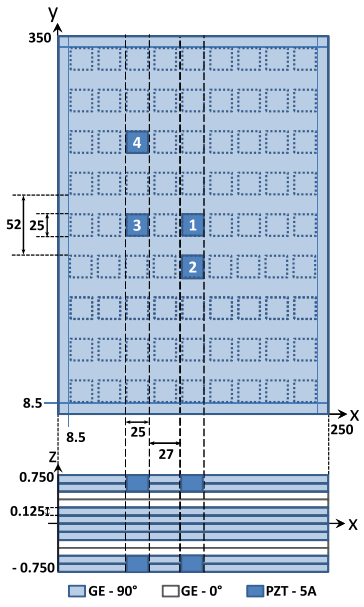

Fig. 3. Schematic representation of the laminate plate with the possible and optimal (highlighted) positions in x- and y-directions for piezoelectric patches.

The EMCC of a given piezoelectric patch/layer used in the evaluations is defined as [29]

$$K_j^2 = \frac{{f_{oc}^j}^2 - {f_{sc}^j}^2}{{f_{oc}^j}^2}, \tag{42}$$

where f_{oc}^j and f_{sc}^j denote the j-th eigenfrequency of the structure evaluated with the analyzed piezoelectric patch/layer in open-circuit and in short-circuit, respectively.

The first four vibration modes are shown in Fig. 4 for piezoelectric patches positioned at the center of the plate. Results have shown that, for all cases, the second position across the thickness gives the best coupling. In this position, the patches external faces coincide with laminate plate external faces, as shown in Fig. 3. For this position in z, the variations of K_j^2 along x- and y-directions are shown in Fig. 5. Notice that, as expected, the optimal position of the patch follows the mode shapes such that the coupling is maximum at the regions of maximum curvature, which are, for instance, at the center of the plate for the first mode. For the second and third vibration modes, two positions of maximum coupling coefficients are available. For the fourth mode, four positions are equally interesting (Fig. 5). Following this analysis, the chosen optimal locations in xy are shown in Fig. 3 labeled according to the vibration mode. The squared modal electromechanical coupling coefficients for these locations are shown in Table 4.

In a second analysis, four pairs of piezoelectric patches are considered, where each pair is considered to focus at one of the four vibration modes and, hence, is located where maximum coupling is obtained for the corresponding vibration mode. The resulting design is defined by considering all highlighted patches in Fig. 3. The coupling coefficients were then evaluated for each vibration mode by making all patches in open circuit or short circuit and are presented in Table 4. It is possible to notice that, although each pair was located to optimize the coupling for only one vibration mode, the second and fourth pairs lead to non-null coupling with vibration modes other than the ones they were designed for.

4.2. Design of resonant shunt circuits

This section presents a simplified formulation based on the theory of dynamic vibration absorbers for the design of a passive shunt circuit working similarly to mechanical vibration absorbers, but using piezoelectric patches as converters of mechanical energy into electrical energy and the shunt circuit as an electrical absorber. For that, the resistance and inductance of the circuit have to be properly tuned to optimize the energy absorption/dissipation. In order to use the standard theory of dynamic vibration absorbers [30], the equations of motion (41) are reduced to two degrees of freedom, one mechanical, corresponding to the modal displacement of one vibration mode of interest, and one electrical,

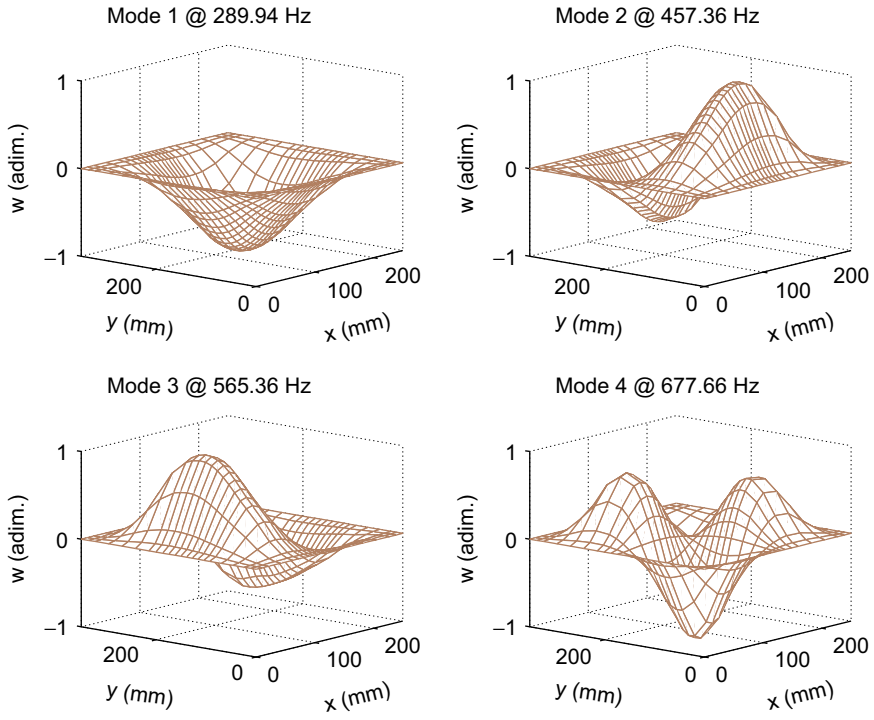

Fig. 4. First four vibration modes for the laminate plate with one symmetrical pair of thickness-poled piezoelectric patches located at the center of the plate.

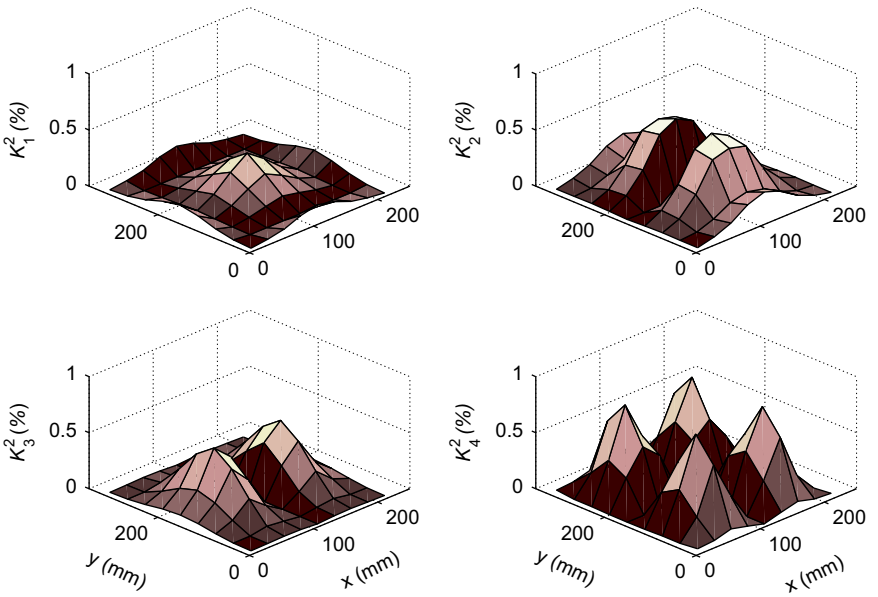

Fig. 5. Variation of the squared modal electromechanical coupling coefficient of a symmetrical pair of piezoelectric patches with their positions along the x- and y-directions.

Table 4
Squared modal electromechanical coupling coefficient K_j^2 (%) for the first four vibration modes provided by the four piezoelectric patch pairs.

Patch pair	Mode j			
	1	2	3	4
1	**0.35**	0.00	0.00	0.00
2	0.23	**0.59**	0.00	0.00
3	0.10	0.00	**0.54**	0.00
4	0.03	0.26	0.22	**0.79**
1–4	1.12	0.54	1.20	1.67

corresponding to the electric charge in the shunt circuit. This simplification implies that one or more piezoelectric patches must be connected to a single shunt circuit and that the contribution of other vibration modes to the structural response is neglected. Therefore, consider the following modal decomposition for the nodal displacements as

$$\mathbf{u}(t) = \boldsymbol{\phi}_n \alpha_n(t), \tag{43}$$

where $\boldsymbol{\phi}_n$ is the mass-normalized vibration mode of interest and α_n is the corresponding modal displacement. Moreover, as only one circuit is considered, the equations of motion (41) are reduced to

$$\ddot{\alpha}_n + \omega_n^2 \alpha_n - k_p q_c = b_n f, \tag{44}$$

$$L_c \ddot{q}_c + R_c \dot{q}_c + \overline{K}_e q_c - k_p \alpha_n = 0, \tag{45}$$

with the following definitions: $k_p = \boldsymbol{\phi}_n^{\mathrm{t}} \overline{\mathbf{K}}_{me}$, $\mathbf{F}_m = \mathbf{b} f$ and $b_n = \boldsymbol{\phi}_n^{\mathrm{t}} \mathbf{b}$. Notice that ω_n is the n-th eigenfrequency of the structure considering open-circuit condition for all piezoelectric patches that are connected to the electric circuit.

In order to evaluate the frequency response function of the structure with piezoelectric patches connected to the electric shunt circuit, let us consider that the structure is excited through a harmonic mechanical force $f = \tilde{f} e^{j\omega t}$, such that $\alpha_n = \tilde{\alpha}_n e^{j\omega t}$ and $q_c = \tilde{q}_c e^{j\omega t}$, and its response is measured by a sensor that gives output $y = \mathbf{cu}$, where $\mathbf{c}$ is a row vector that defines the degree of freedom that is measured. Hence, $y = \tilde{y} e^{j\omega t}$, where $\tilde{y} = c_n \tilde{\alpha}_n$ and $c_n = \mathbf{c}\boldsymbol{\phi}$. The equations of motion (44) and (45) then become

$$(\omega_n^2 - \omega^2)\tilde{\alpha}_n - k_p \tilde{q}_c = b_n \tilde{f}, \tag{46}$$

$$(-\omega^2 L_c + j\omega R_c + \overline{K}_e)\tilde{q}_c - k_p \tilde{\alpha}_n = 0. \tag{47}$$

Solving (47) for $\tilde{q}_c$ and substituting in (46), it is possible to write $\tilde{\alpha}_n$ and, thus $\tilde{y}$, in terms of the excitation amplitude $\tilde{f}$, such that $\tilde{y} = G_p(\omega)\tilde{f}$, where $G_p(\omega)$ is the frequency response function of the structure, subjected to a mechanical excitation, which results in

$$G_p(\omega) = c_n b_n \frac{-\omega^2 L_c + \overline{K}_e + j\omega R_c}{\omega^4 L_c - \omega^2(\overline{K}_e + \omega_n^2 L_c) + \omega_n^2 \overline{K}_e - k_p^2 + j\omega R_c(\omega_n^2 - \omega^2)}. \tag{48}$$

The amplitude of the frequency response function is written as

$$|G_p(\omega)| = c_n b_n \sqrt{\frac{(-\omega^2 L_c + \overline{K}_e)^2 + (\omega R_c)^2}{[\omega^4 L_c - \omega^2(\overline{K}_e + \omega_n^2 L_c) + \omega_n^2 \overline{K}_e - k_p^2]^2 + [\omega R_c(\omega_n^2 - \omega^2)]^2}}, \tag{49}$$

which, for limited values of R_c, can be shown to have an anti-resonance at a frequency equal to the resonance frequency of the electric circuit, defined as $\omega_c = (\overline{K}_e/L_c)^{1/2}$. One strategy to minimize the vibration amplitude of the structure at a resonance frequency of interest is to design the resonance frequency of the secondary system, the shunt circuit in the present case, such that it coincides with the resonance frequency of interest of the primary system, i.e. the structure. Therefore, the following identity is defined as $\omega_c = \omega_n$, which allows to evaluate directly the inductance of the shunt circuit as

$$L_c = \frac{\overline{K}_e}{\omega_n^2}. \tag{50}$$

Nevertheless, the designed anti-resonance at ω_n is accompanied by two resonances, before and after ω_n, which must have their amplitude controlled to minimize or prevent amplification of the original vibration amplitude. This can be done using the resistance parameter of the shunt circuit. One possible methodology based on the dynamic vibration absorbers theory [30] is to design the damping parameter, which is the shunt circuit resistance, such that the amplitude at the anti-resonance is approximately equal to that at one of the two invariant frequencies, which are independent of the damping parameter, found by the following relation:

$$\lim_{R_c \to 0} |G_p(\omega)|^2 = \lim_{R_c \to \infty} |G_p(\omega)|^2, \tag{51}$$

leading to

$$\omega_{1,2}^2 = \frac{1}{2}[\omega_c^2 + \omega_n^2 \pm \sqrt{(\omega_c^2 - \omega_n^2)^2 + 2\omega_c^2(k_p^2/\overline{K}_e)}]. \tag{52}$$

Hence, the vibration amplitudes at one of these invariant frequencies ω_1 and at the anti-resonance frequency ω_n are evaluated, leading to

$$|G_p(\omega_1)|^2 = \frac{R_c^2 \omega_n^2}{k_p^4} \quad \text{and} \quad |G_p(\omega_n)|^2 = \frac{2\overline{K}_e}{k_p^2 \omega_n^2}, \tag{53}$$

and, then, equalized such that the following expression for the resistance R_c can be found in terms of the equivalent coupling stiffness k_p, electrical stiffness $\overline{K}_e$ and structural resonance frequency of interest ω_n,

$$R_c = \frac{k_p \sqrt{2\overline{K}_e}}{\omega_n^2}. \tag{54}$$

4.3. Performance results for passive vibration control using resonant circuits

The methodology presented in the previous section was then applied to the clamped laminate composite plate with symmetrical pairs of piezoelectric patches represented in Fig. 3. Each pair is considered to be connected to a resonant shunt circuit, for which the resistance and inductance are evaluated according to the expressions (50) and (54) using the corresponding eigenfrequencies ω_n and eigenmodes $\boldsymbol{\phi}_n$.

The frequency response functions for the laminate plate were evaluated considering five cases and using 600 plate elements. For the first four cases, a single pair of piezoelectric patches, located to properly couple with one of the first four vibration modes according to Fig. 3, is considered. For the last case, the four pairs of piezoelectric patches are embedded simultaneously in the laminate plate and connected to the corresponding resonant shunt circuit to yield a multi-modal vibration reduction. In all cases, the frequency response function of the laminate plate with shunted piezoelectric patches was compared to the case of open-circuit condition to analyze the performance of vibration amplitude reduction. For comparison purposes, a modal damping of 0.5% was considered for the host structure.

However, a preliminary analysis showed, for most cases, that the location of the anti-resonance and the amplitude of the resonances generated by the shunt circuit were not exactly as expected. Therefore, some variations in the values of R_c and L_c, starting from the values obtained by the expressions (50) and (54), were tested and, indeed, better results were found with an update of these values. The update was performed manually respecting the following known properties: (i) the anti-resonance frequency must coincide with the structure's resonance frequency of interest and its value is

inversely proportional to the square root of L_c, thus L_c was augmented when the anti-resonance frequency was larger than expected and vice-versa; and (ii) as long as there are two resonances generated by the resonant shunt circuit, their amplitude can be reduced by increasing the resistance, and, if there is only resonance, the resistance may be larger than the value which makes the two resonances converge into one and, thus, must be diminished. Table 5 shows the calculated and updated values of R_c and L_c for each circuit in the cases of one and four pairs of piezoelectric patches. It is possible to observe that the values of L_c were slightly changed, while the values of R_c were greatly changed in most cases, except for the first mode-patch. This indicates that the one degree of freedom approximation for the evaluation R_c is not appropriate for frequency regions with higher modal density. Therefore, the expression (54) should be used with caution or else be used as an initial guess for a manual or automatic optimization procedure.

Then, considering the updated values for R_c and L_c, a first analysis is performed considering that only one pair of piezoelectric patches is embedded in the laminate plate and connected to a resonant shunt circuit. This is done for all four pairs of piezoelectric patches presented in Fig. 3, one at a time. The frequency response function of the structure with one shunted pair of piezoelectric patches (RL) is evaluated and compared to the case of open-circuit (OC) piezoelectric patches ($R_c=\infty$ and L_c=0). The comparative results are presented in Figs. 6–9 for the first, second, third and fourth patch pairs—vibration modes. In all cases, the vibration amplitude is only significatively modified near the resonance frequency considered in the positioning and circuit design. However, it is possible to observe that the fourth shunted patch pair, which was designed for the fourth vibration mode, also affects slightly the second and fifth vibration modes. Therefore, this technique may yield an adequate vibration reduction with a narrow frequency-range performance. The amount of amplitude reduction for each case is presented in Table 6, where one may observe that all shunted patch pairs are able to reduce the vibration amplitude at the selected resonance frequency by more than 10 dB. This value was evaluated from the difference between the amplitude at resonance for the open-circuit case and the higher amplitude between the two resonances for the shunted case.

A second analysis is performed considering that the four pairs of piezoelectric patches are embedded simultaneously in the laminate plate and connected to the corresponding resonant shunt circuit to evaluate the case of a multi-modal vibration reduction. Notice that in this case, the eigenfrequencies and eigenmodes are different from the previous case and, thus, the resistances and inductances need to be reevaluated and also updated according to Table 5. Fig. 10 shows the

Table 5
Values for R_c and L_c calculated using (50) and (54) and updated after simulations.

Circuit	1 pair of PZT patches				4 pairs of PZT patches			
	R_c (Ω)		L_c (H)		R_c (Ω)		L_c (H)	
	Calculated	Updated	Calculated	Updated	Calculated	Updated	Calculated	Updated
1	987	988	6.30	6.20	678	650	5.13	5.11
2	104	730	1.99	1.99	136	310	1.93	1.94
3	375	350	1.48	1.44	306	468	1.54	1.47
4	133	280	0.97	0.96	63	580	1.02	0.98

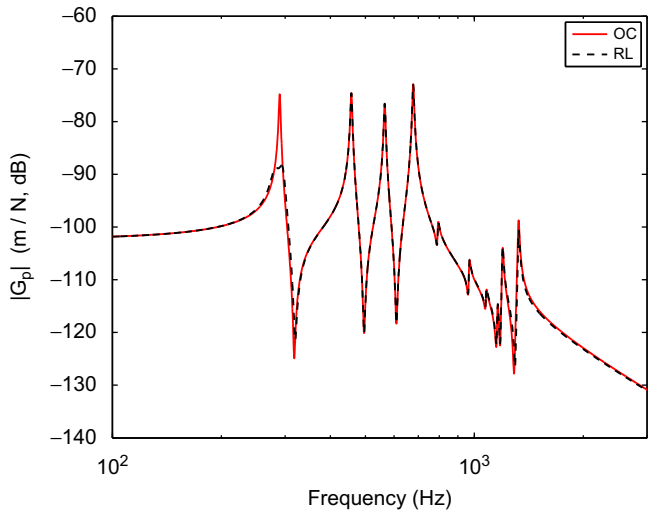

Fig. 6. Frequency response function of the laminate plate with one pair of shunted piezoelectric patches designed for the first vibration mode.

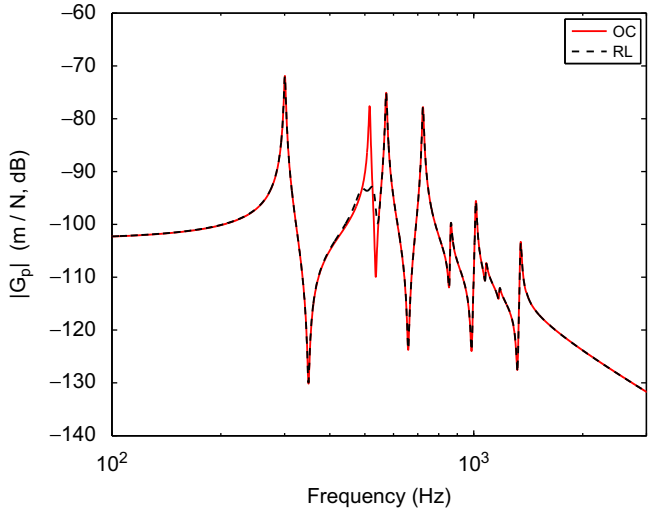

Fig. 7. Frequency response function of the laminate plate with one pair of shunted piezoelectric patches designed for the second vibration mode.

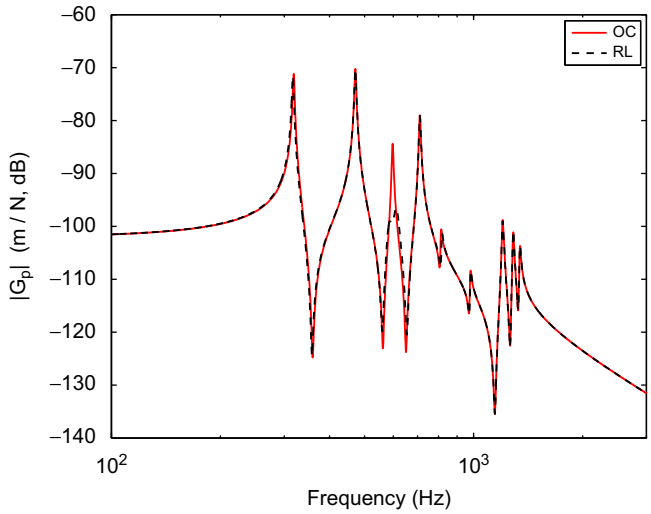

Fig. 8. Frequency response function of the laminate plate with one pair of shunted piezoelectric patches designed for the third vibration mode.

frequency response function of the laminate plate with four pairs of piezoelectric patches, distributed according to Fig. 3, in two electrical boundary conditions: (i) all patches in open-circuit (OC) and (ii) each pair of patches connected to a properly designed resonant shunt circuit, focusing one of the four first vibration modes. It is possible to observe in Fig. 10 that the vibration amplitude at the first four resonance frequencies is effectively reduced by the shunted piezoelectric patches, especially for the fourth resonance. In addition, the vibration amplitude at the fifth resonance, which was not included in the design, is also slightly reduced. Similarly to the previous case, the amount of amplitude reduction, based on the difference between the peak amplitudes, was evaluated and is presented in Table 6. In this case, a vibration amplitude reduction of more than 10 dB is also observed, but for the first four vibration modes simultaneously.

5. Control authority enhancement using RL shunts

As an extension of the use of shunt circuits connected to piezoelectric elements for passive vibration control, it is also possible to include a voltage source to these circuits so that the piezoelectric elements may act both as vibration dampers/absorbers and actuators. Hence, passive, active and active–passive vibration control could be obtained. In the particular case of the circuit proposed previously, composed of resistance, inductance and voltage source, it is worthwhile to analyze

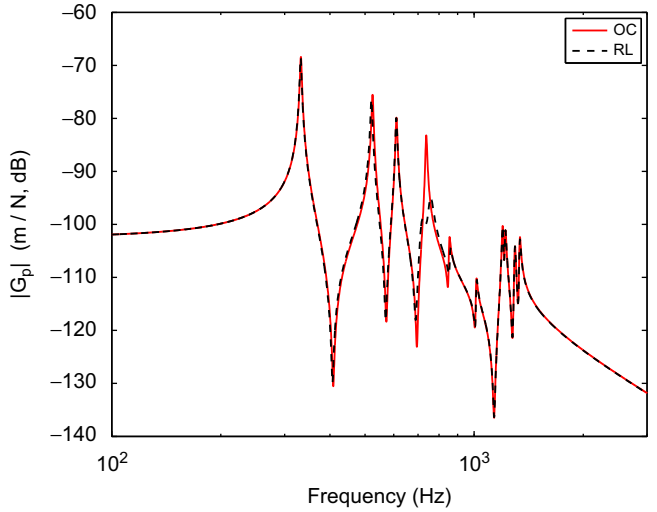

Fig. 9. Frequency response function of the laminate plate with one pair of shunted piezoelectric patches designed for the fourth vibration mode.

Table 6
Vibration amplitude reduction (dB), from the open-circuit case, for the laminate plates with 1 and 4 pairs of shunted piezoelectric patches.

Mode	1 pair of PZT patches	4 pairs of PZT patches
1	13.50	12.24
2	15.24	11.11
3	12.19	14.36
4	11.72	16.84

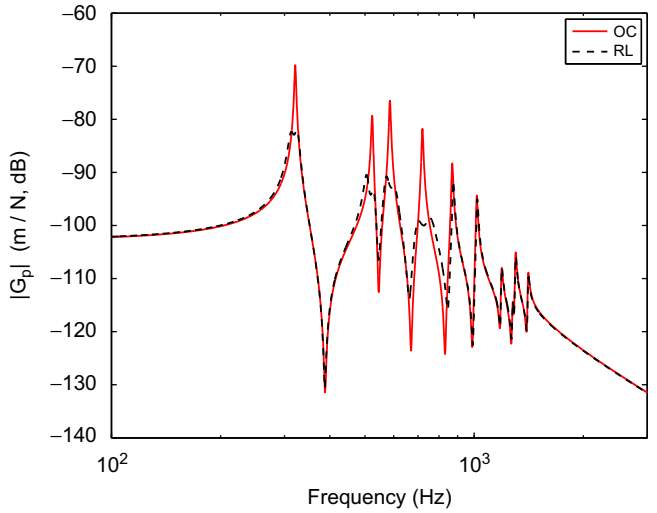

Fig. 10. Frequency response function of the laminate plate with four pairs of shunted piezoelectric patches designed for the first four vibration modes.

the active and active–passive action, since the passive action is obtained by eliminating the voltage source, which is the case treated in previous section.

5.1. Evaluation of control authority of piezoelectric actuators

To evaluate the active action (control authority) of the piezoelectric elements, through a RL circuit, a harmonic excitation analysis is performed considering excitation through a single voltage source, that is a single piezoelectric

element connected to a circuit composed of resistance, inductance and voltage source, such that

$$\mathbf{F}_m = 0, \quad \mathbf{V}_c = \tilde{V}_c e^{j\omega t}, \quad \mathbf{u} = \tilde{\mathbf{u}} e^{j\omega t}, \quad \mathbf{q}_c = \tilde{q}_c e^{j\omega t}, \tag{55}$$

and, thus, the equations of motion (41) can be rewritten as

$$(-\omega^2 \mathbf{M} + \mathbf{K}_m)\tilde{\mathbf{u}} - \overline{\mathbf{K}}_{me}\tilde{q}_c = \mathbf{0},$$

$$-\overline{\mathbf{K}}_{me}^{t}\tilde{\mathbf{u}} + (-\omega^2 L_c + j\omega R_c + \overline{K}_e)\tilde{q}_c = \tilde{V}_c. \tag{56}$$

Solving the second equation of (56) for $\tilde{q}_c$ and replacing the solution in the first equation leads to

$$[-\omega^2 \mathbf{M} + \mathbf{K}_m - \overline{\mathbf{K}}_{me}(-\omega^2 L_c + j\omega R_c + \overline{K}_e)^{-1}\overline{\mathbf{K}}_{me}^{t}]\tilde{\mathbf{u}} = \overline{\mathbf{K}}_{me}(-\omega^2 L_c + j\omega R_c + \overline{K}_e)^{-1}\tilde{V}_c. \tag{57}$$

To evaluate the frequency response function of the structure subjected to an electrical excitation, it is supposed that a selected displacement in the structure is measured, such that

$$\tilde{y} = \mathbf{c}\tilde{\mathbf{u}}, \tag{58}$$

and the complex frequency response function of the displacement output when subjected to the voltage input can be defined as

$$\tilde{y} = G_c(\omega)\tilde{V}_c, \tag{59}$$

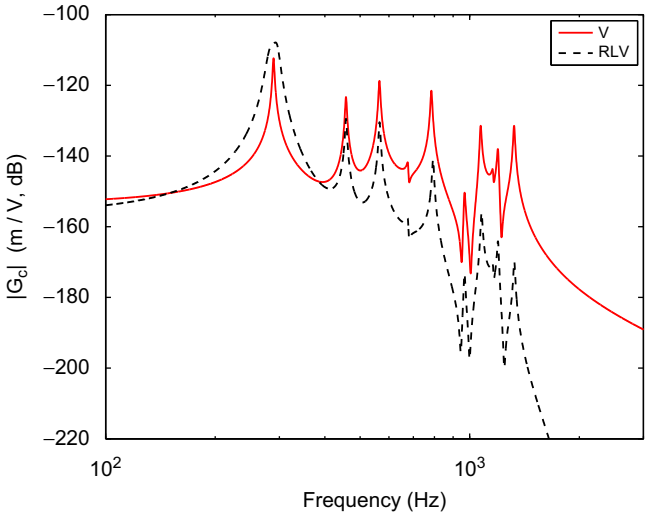

Fig. 11. Control authority of the first pair of piezoelectric patches with (RLV) and without (V) resonant circuit.

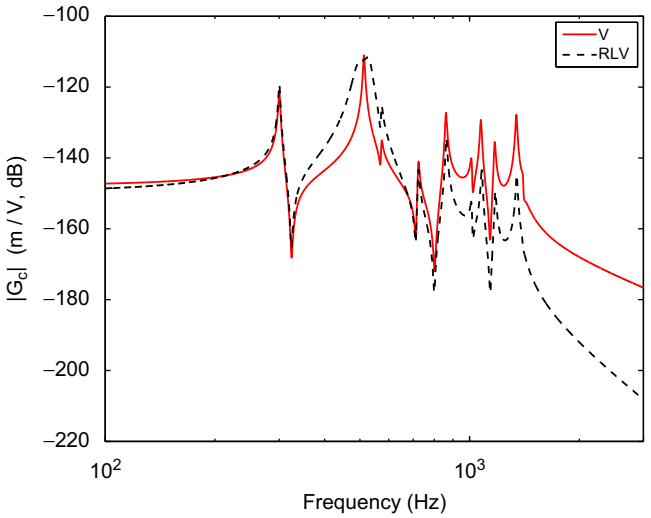

Fig. 12. Control authority of the second pair of piezoelectric patches with (RLV) and without (V) resonant circuit.

where

$$G_c(\omega) = \mathbf{c}[-\omega^2\mathbf{M} + \mathbf{K}_m - \overline{\mathbf{K}}_{me}(-\omega^2 L_c + \mathrm{j}\omega R_c + \overline{K}_e)^{-1}\overline{\mathbf{K}}_{me}^{\mathrm{t}}]^{-1}\overline{\mathbf{K}}_{me}(-\omega^2 L_c + \mathrm{j}\omega R_c + \overline{K}_e)^{-1}. \tag{60}$$

As in the passive case studied previously, the resistance and inductance of the electric circuits lead to a modification of the dynamic stiffness of the piezoelectric elements. The purely active case can be represented by considering $L_c = R_c = 0$. In this case, the frequency response function reduces to

$$G_c^V(\omega) = \mathbf{c}[-\omega^2\mathbf{M} + \mathbf{K}_m - \overline{\mathbf{K}}_{me}\overline{K}_e^{-1}\overline{\mathbf{K}}_{me}^{\mathrm{t}}]^{-1}\overline{\mathbf{K}}_{me}\overline{K}_e^{-1}, \tag{61}$$

where $\overline{\mathbf{K}}_{me}\overline{K}_e^{-1}$ indicates the equivalent force vector induced per unit voltage applied to the actuator and the reduction of piezoelectric stiffness accounts for the modification from a constant electric displacement to a constant electric field condition. The open-circuit case ($R_c \to \infty$) leads to the impossibility of actuation as expected.

For the most general case, the inductance and resistance not only modify the dynamic stiffness of the piezoelectric element, leading to vibration damping and/or absorption, but also affect the active control authority of the actuator due to the term $\overline{\mathbf{K}}_{me}(-\omega^2 L_c + \mathrm{j}\omega R_c + \overline{K}_e)^{-1}$ in (60). In particular, it may be possible to amplify the active control authority near the resonance frequency of the electric circuit [8,31,32].

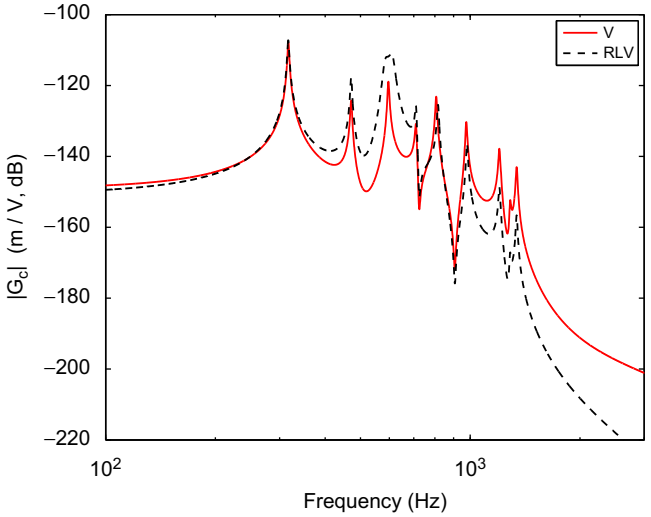

Fig. 13. Control authority of the third pair of piezoelectric patches with (RLV) and without (V) resonant circuit.

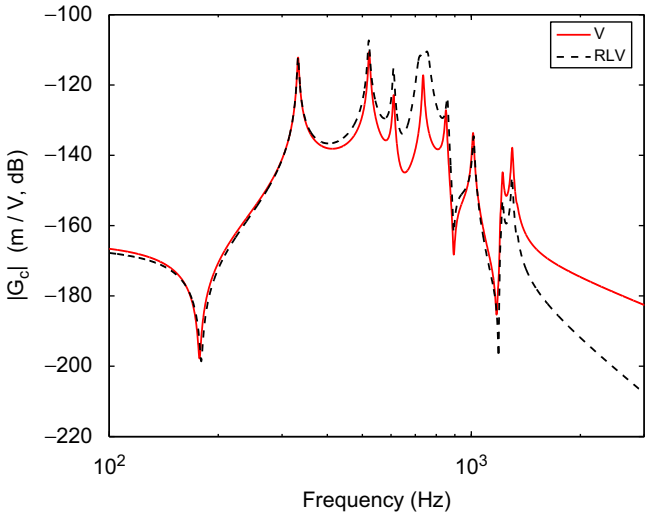

Fig. 14. Control authority of the fourth pair of piezoelectric patches with (RLV) and without (V) resonant circuit.

5.2. Results for a laminate plate with piezoelectric actuators

In this section, the same laminate composite plate with four pairs of piezoelectric patches from the passive vibration control study is considered to evaluate the control authority of the piezoelectric patches, when they are used to excite the plate. This is done adding a voltage source in each one of the independent electric circuits connected to the pair of piezoelectric patches. To allow the analysis of the control authority enhancement provided by the RL elements of the circuit, the control authority $G_c(\omega)$ of a piezoelectric patch when connected to an electric circuit with resistance, inductance and voltage source (RLV) is compared to the one obtained with a piezoelectric patch connected to an electric circuit with only voltage source (V), $G_c^V(\omega)$, that is considering $L_c=R_c=0$. This analysis is performed for each one of the four pair of piezoelectric patches, considering first only one pair of piezoelectric patches embedded into the plate and then with the four pairs of piezoelectric patches simultaneously.

Figs. 11–14 present the control authority of each one of the four pairs of piezoelectric patches, connected to RLV circuits tuned to the first four resonances, when only the active pair is embedded into the structure. In Fig. 11, it is easy to notice that the control authority around the first resonance frequency is indeed enhanced at the cost of reducing the control

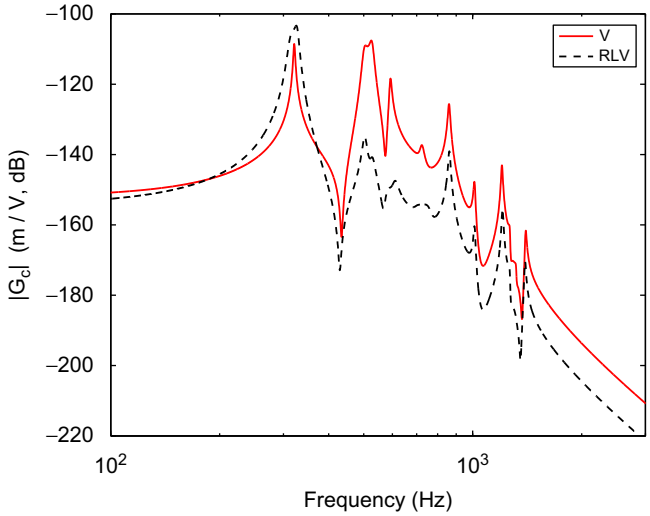

Fig. 15. Control authority of the first pair of piezoelectric patches with (RLV) and without (V) resonant circuit when the other three pairs are connected to a passive RL circuit.

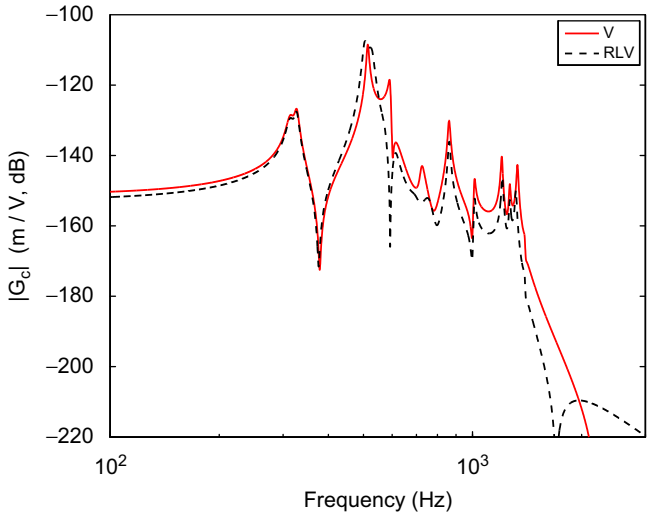

Fig. 16. Control authority of the second pair of piezoelectric patches with (RLV) and without (V) resonant circuit when the other three pairs are connected to a passive RL circuit.

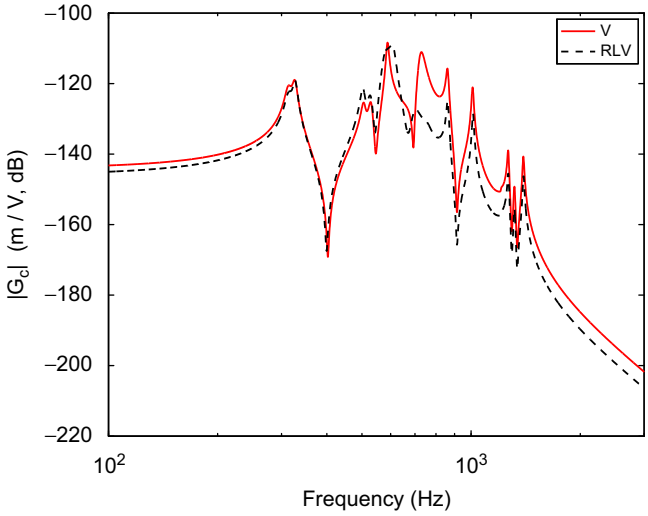

Fig. 17. Control authority of the third pair of piezoelectric patches with (RLV) and without (V) resonant circuit when the other three pairs are connected to a passive RL circuit.

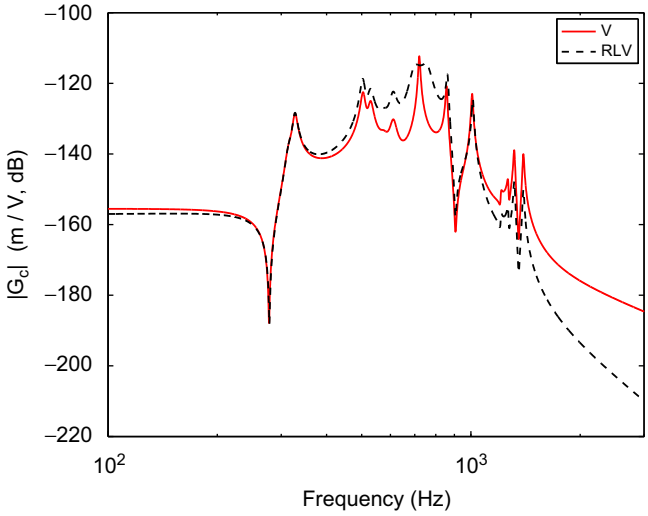

Fig. 18. Control authority of the fourth pair of piezoelectric patches with (RLV) and without (V) resonant circuit when the other three pairs are connected to a passive RL circuit.

authority at other frequencies. Unlike previous results published in the literature [8,33], for this case the control authority is enhanced even exactly at the first resonance frequency and not only around it. For the other three cases (Figs. 12–14), it becomes evident that the resonant circuit amplifies the control authority for a certain frequency range around the chosen resonance frequency. Indeed, for the third pair presented in Fig. 13, the control authority is enhanced for the second, third and fourth resonance frequencies, although more effectively for the third one as expected. It should also be noticed that the location of the piezoelectric patch also affects the control authority. For instance, the second pair is not effective for controlling the third and fourth modes, even through the resonant circuit (Fig. 12).

Figs. 15–18 present the control authority of each one of the four pairs of piezoelectric patches, connected to RLV circuits tuned to the first four resonances, when the four pairs are embedded into the structure but only one of them is active. In this case, the inactive pairs are considered to be connected to a passive RL shunt circuit, that is without the voltage source. In this case, the control authority enhancement is still possible, but it can be noticed, in particular for the second and third pairs (Figs. 16 and 17), that the passive circuits may affect the control authority of the active circuit. As an alternative analysis for simultaneous action of the four pairs, Fig. 19 presents the control authority of the four pairs of piezoelectric patches, connected to RLV circuits tuned to the first four resonances, when the four pairs are embedded into the structure and connected to the same voltage source. In this case, it is possible to observe an enhancement on the control authority of the four pairs simultaneously.

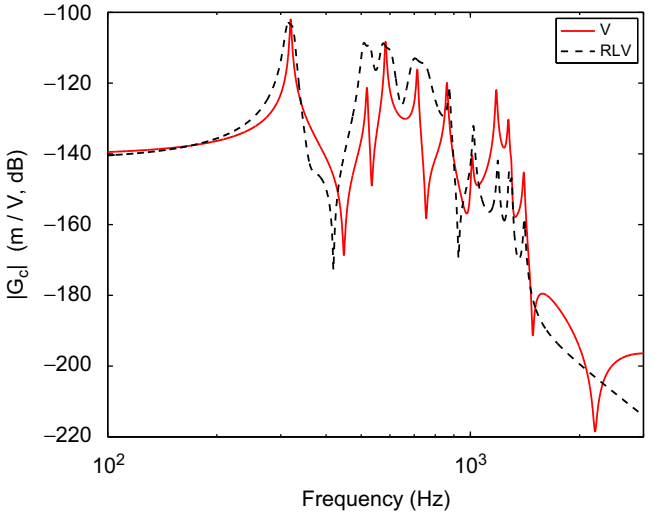

Fig. 19. Control authority of the four pairs of piezoelectric patches with (RLV) and without (V) resonant circuit when acting simultaneously.

6. Conclusions

The finite element modeling of laminate composite plates with embedded piezoelectric patches or layers connected to active–passive resonant shunt circuits, composed of resistance, inductance and voltage source, was presented. Applications to passive vibration control and active control authority enhancement were studied and discussed. An equivalent single layer theory combined with a third-order shear deformation theory was considered for the laminate plate and a stress-voltage electromechanical model was considered for the piezoelectric materials. Also, the dynamics of the electric circuits connected to piezoelectric materials were accounted for resulting in a coupled finite element model with mechanical (displacements) and electrical (charges at electrodes) degrees of freedom. The model was then used to optimize the location of a set of piezoelectric patches, using the electromechanical coupling coefficient, and design the electric circuit components for optimal passive vibration control and active control authority enhancement. A passive vibration amplitude reduction of at least 10 dB for the first four vibration modes was obtained. It was also shown that the control authority can indeed be improved near a selected resonance even with multiple pairs of piezoelectric patches and active–passive circuits acting simultaneously.

Acknowledgments

This research was supported by FAPESP and CNPq, through research Grants 04/10255-7 and 473105/2004-7, which the authors gratefully acknowledge. The first author acknowledges CAPES for a graduate scholarship. The authors also acknowledge the support of the MCT/CNPq/FAPEMIG National Institute of Science and Technology on Smart Structures in Engineering, Grant no. 574001/2008-5.

References

[1] M. Sunar, S. Rao, Recent advances in sensing and control of flexible structures via piezoelectric materials technology, *Applied Mechanics Review* 52 (1) (1999) 1–16.
[2] M. Schultz, M. Hyer, R. Brett Williams, W. Keats Wilkie, D. Inman, Snap-through of unsymmetric laminates using piezocomposite actuators, *Composites Science and Technology* 66 (2006) 2442–2448.
[3] C. Bowen, R. Butler, R. Jervis, H. Kim, A. Salo, Morphing and shape control using unsymmetrical composites, *Journal of Intelligent Material Systems and Structures* 18 (2007) 89–98.
[4] M. Ahmadian, A. DeGuilio, Recent advances in the use of piezoceramics for vibration suppression, *The Shock and Vibration Digest* 33 (1) (2001) 15–22.
[5] R. Forward, Electronic damping of vibrations in optical structures, *Applied Optics* 18 (5) (1979) 690–697.
[6] N. Hagood, A. von Flotow, Damping of structural vibrations with piezoelectric materials and passive electrical networks, *Journal of Sound and Vibration* 146 (2) (1991) 243–268.
[7] J. Tang, Y. Liu, K. Wang, Semiactive and active-passive hybrid structural damping treatments via piezoelectric materials, *The Shock and Vibration Digest* 32 (3) (2000) 189–200.
[8] M. Tsai, K. Wang, On the structural damping characteristics of active piezoelectric actuators with passive shunt, *Journal of Sound and Vibration* 221 (1) (1999) 1–22.
[9] D. Saravanos, P. Heyliger, D. Hopkins, Layerwise mechanics and finite element for the dynamic analysis of piezoelectric composite plates, *International Journal of Solids and Structures* 34 (3) (1997) 359–378.
[10] S. Gopinathan, V. Varadan, V. Varadan, A review and critique of theories for piezoelectric laminates, *Smart Materials and Structures* 9 (2000) 24–48.

[11] D. Saravanos, P. Heyliger, Mechanics and computational models for laminated piezoelectric beams, plates, and shells, *Applied Mechanics Review* 52 (10) (1999) 305–320.
[12] S. Vel, R. Batra, Three-dimensional analytical solution for hybrid multilayered piezoelectric plates, *Journal of Applied Mechanics* 67 (2000) 558–567.
[13] A. Benjeddou, Advances in piezoelectric finite elements modeling of adaptive structural elements: a survey, *Computers and Structures* 76 (1–3) (2000) 347–363.
[14] B. Baillargeon, S. Vel, Active vibration suppression of sandwich beams using piezoelectric shear actuators: experiments and numerical simulations, *Journal of Intelligent Material Systems and Structures* 16 (6) (2005) 517–530.
[15] J.-F. Deü, A. Benjeddou, Free-vibration analysis of laminated plates with embedded shear-mode piezoceramic layers, *International Journal of Solids and Structures* 42 (7) (2005) 2059–2088.
[16] E. Carrera, Assessment of theories for free vibration analysis of homogeneous and multilayered plates, *Shock and Vibration* 11 (2004) 261–270.
[17] J. Reddy, On laminated composite plates with integrated sensors and actuators, *Engineering Structures* 21 (1999) 568–593.
[18] M. Trindade, A. Benjeddou, On higher-order modelling of smart beams with embedded shear-mode piezoceramic actuators and sensors, *Mechanics of Advanced Materials and Structures* 13 (5) (2006) 357–369.
[19] M. Trindade, A. Benjeddou, Refined sandwich model for the vibration of beams with embedded shear piezoelectric actuators and sensors, *Computers and Structures* 86 (9) (2008) 859–869.
[20] O. Aldraihem, A. Khdeir, Analytical solutions of antisymmetric angle-ply laminated plates with thickness-shear piezoelectric actuators, *Smart Materials and Structures* 15 (2006) 232–242.
[21] A. Benjeddou, J.-F. Deü, A two-dimensional closed-form solution for the free-vibrations analysis of piezoelectric sandwich plates, *International Journal of Solids and Structures* 39 (2002) 1463–1486.
[22] R. Thornburgh, A. Chattopadhyay, Simultaneous modeling of mechanical and electrical response of smart composite structures, *AIAA Journal* 40 (8) (2002) 1603–1616.
[23] R. Thornburgh, A. Chattopadhyay, A. Ghoshal, Transient vibration of smart structures using a coupled piezoelectric-mechanical theory, *Journal of Sound and Vibration* 274 (1–2) (2004) 53–72.
[24] A. Benjeddou, M. Trindade, R. Ohayon, New shear actuated smart structure beam finite element, *AIAA Journal* 37 (3) (1999) 378–383.
[25] T. Godoy, Modeling of Laminate Plates with Piezoelectric Materials Connected to Resistive–inductive Shunt Circuits, Master's Thesis, São Carlos School of Engineering, University of São Paulo, São Carlos, 2008 (in Portuguese).
[26] V. Franco Correia, M. Aguiar Gomes, A. Suleman, C. Mota Soares, C. Mota Soares, Modelling and design of adaptive composite structures, *Computer Methods in Applied Mechanics and Engineering* 185 (2–4) (2000) 325–346.
[27] B. Baillargeon, S. Vel, Exact solution for the vibration and active damping of composite plates with piezoelectric shear actuators, *Journal of Sound and Vibration* 282 (2005) 781–804.
[28] M. Trindade, A. Benjeddou, R. Ohayon, Finite element modeling of hybrid active-passive vibration damping of multilayer piezoelectric sandwich beams—part 2: system analysis, *International Journal for Numerical Methods in Engineering* 51 (7) (2001) 855–864.
[29] M. Trindade, A. Benjeddou, Effective electromechanical coupling coefficients of piezoelectric adaptive structures: critical evaluation and optimization, *Mechanics of Advanced Materials and Structures* 16 (3) (2009) 210–223.
[30] J. Den Hartog, *Mechanical Vibrations*, McGraw-Hill, New York, 1947.
[31] C. Niezrecki, H. Cudney, Improving the power consumption characteristics of piezoelectric actuators, *Journal of Intelligent Material Systems and Structures* 5 (4) (1994) 522–529.
[32] J. Sirohi, I. Chopra, Actuator power reduction using l-c oscillator circuits, *Journal of Intelligent Material Systems and Structures* 12 (12) (2001) 867–877.
[33] H. Santos, M. Trindade, Vibration control using extension and shear active-passive piezoelectric networks subject to parametric uncertainties, *Proceedings of the XIII International Symposium on Dynamic Problems of Mechanics* (*DINAME 2009*), ABCM, Rio de Janeiro, 2009.